Revista Mexicana de Física **35** *No. 4(1989) 552-596*

Some aspects of radiationless energy transfer between impurity ions in ionic solids

Julio Rubio O.

Departamento de Física, Universidad Autónoma Metropolitana-Iztapalapa
Apartado postal 55-534, 09340 México, D.F.

(Recibido el 11 de mayo de 1989; aceptado el 5 de junio de 1989)

Abstract. The phenomenon of radiationless energy transfer between impurities in solids is one of the fundamental problems in modern physics of condensed matter, in view of its importance in technological applications. In this paper, it's presented a review of the most significant experimentally determined data obtained by the present author and his collaborators in this research field. It is shown that some impurites, depending on the crystalline host, tend to form close pairs in which an efficient radiationless energy transfer process can take place. This preferential impurity pairing, which has been traditionally considered to be unfrequently might help to design more efficient devices for the optical convertion of ultraviolet or infrared light into visible light. In order to explain this preferential impurity pairing, Rubio *et al.* have proposed an ionic radius criterion which appears to be quite useful to select impurity ions and host materials, where we want to produce an efficient energy transfer.

PACS: 78.55.Fv

1. Introduction

The sensitized luminescence of phosphors, first discovered by Rothschild [1] in 1934, has been the subject of a considerable number of investigations up to date. The interest displayed in this research field is due partly to its practical applications and partly to the theoretical problems that arise as a consequence of the transport and transfer of energy in the solid material.

Electronic excitation energy transfer in solids is one of the fundamental problems in modern physics of condensed matter. This is a fairly universal problem since transfer of electronic excitation energy is an intermediate process between the primary event of electronic excitation and the final processes that use the energy of electrons. Therefore, the analysis of the mechanisms of electronic energy transfer, and in particular, the analysis of their efficiency are indispensable in the studies of the interaction between various types of radiation and matter when what is studied is not only the absorption of radiation energy but also the accompanying effects on the absorbing medium.

Electronic excitation energy transfer plays an essential role in modern research fields such as luminescence, radiation physics, radiation chemistry, photosynthesis, biochemistry, bioenergetics, etc. This generality has made energy transfer an important topic for study by physicists, chemists, and biologists with many different special research interests.

Sensitized fluorescence involves two centers or ions; the sensitizer or donor and the acceptor or activator. Generally, the acceptor ion provides an emission band in a desired spectral region of the electromagnetic spectrum but does not absorb radiation, efficiently, in the excitation range of interest. On the other hand, the donor ion possesses an absorption band in the required excitation range, and if it is present alone in the solid material, will fluoresce with its characteristic emission spectrum. When both the donor and acceptor ions are present in a coactivated phosphor material, the donor ion will transfer part of its excitation energy to the acceptor ion causing a fluorescence spectrum, which is a characteristic of the latter. The total fluorescence spectrum of the coactivated phosphor is thus a composite of the emission of both the donor and acceptor ions. The relative intensities of these two emissions are strongly dependent on the respective ion concentrations.

There are three basic mechanisms by which energy transfer may occur in a solid material. The first one arises as a consequence of the creation of free electron-hole pairs by the incident radiation. These pairs can migrate in the solid carrying with them both energy and charge. This mechanism is closely related to the phenomenon of photoconductivity. The second basic mechanism of energy transfer is called "radiative reabsorption". In this mechanism, the donor ion, after being in an excited state, emits a real photon which is eventually absorbed by another donor ion or an acceptor. It is well known that radiative processes depend critically on sample size and experimental configuration and are expected to take place when the acceptor ion has allowed optical absorption transitions. The third basic mechanism is called "radiationless energy transfer" in the absence of charge migration. In this case, the transfer of excitation energy between donor and acceptor ions can be visualized as a quantum mechanical resonance process involving the exchange of a virtual photon. The method by which this process may occur can be through of as an electrostatic multipole-multipole interaction or an exchange interaction between the donor and acceptor ions. Of all this three basic mechanisms of energy transfer between impurities in solid materials, the third one is the most important one in technological applications of optical materials such as enhancing the pumping efficiency of laser systems.

The main objective of the present paper is to summarize some of the more important aspects of radiationless energy transfer between impurities in solids and to present the most significant experimentally determined data on this research field obtained by the present author and his collaborators during the last four years.

2. Theoretical background of radiationless energy transfer

Förster [2–4] was the first one to put forward a satisfactory theory of energy transfer for molecules having broad optical spectra in a condensed medium. This theory was based on perturbation theory in the adiabatic approximation. The theory assumes that energy transfer occurs owing to the weak dipole-dipole interaction between molecules. The interaction is assumed to be so weak that it does not change the initial optical spectra of the molecules. Förster showed that under these conditions the probability of energy transfer can indeed, be expressed in terms of the integral of the overlap of the luminescence and absorption spectra of the interacting molecules. Moreover, Förster was the first to average the probability of transfer over the molecules in the solid solution obtaining relationships which could be compared with the experimentally determined data. The Förster theory is quite useful since its predictions are in good agreement with the experimental data when the conditions for its applicability are met.

Later on, Dexter [5] generalized Förster theory and applied it to the cases of multipole and exchange interactions. Subsequently, the theory was developed to take into account various complicated factors such as the diffusion of molecules during the lifetime of the excited state.

Since Förster's theory is an approximate one, the limits of its applicability have been repeatedly discussed. For instance, Galanin [6–7] derived Förster's theory in the framework of the classical model of two dipole oscillators with friction only under the assumption that the acceptor excitation lifetime is much shorter than the time of the reverse transfer. Robinson and Frosch [8–9] obtained a similar result for a quantum mechanical model. Förster [10] himself discussed the conditions for applicability of his theory. He developed a classification of interaction types according to which his initial theory corresponds to the case of the very weak coupling. The limits of applicability of Förster's theory were also discussed in several papers coming from the density matrix approach [11–13]. These works have led to the best understanding of the role played by the relaxation processes in the transfer phenomena and formulated clear-cut criteria of applicability of various approximations.

The theory of luminescence energy transfer between donor and acceptor ions in solids has been presented in several excellent papers [14–24]. For this reason and also for the sake of brevity, in this paper only those theoretical expressions which are of importance to make a clear interpretation of the experimentally determined data given in section 3 will be summarized.

According to Dexter's theory, the transfer rate for the electric dipole-dipole (DD) interaction between a donor (D) ion and an acceptor (A) ion in a solid material is given by

$$W_{\mathrm{DA}}(\mathrm{DD}) = \frac{3\hbar^4 c^4 Q_{\mathrm{A}}}{4\pi R_{\mathrm{DA}}^6 n^4 \tau_{[\mathrm{D}}^0} \left(\frac{\epsilon}{k^{1/2}\epsilon_c}\right)^4 \int \frac{F_{\mathrm{D}}(E) F_{\mathrm{A}}(E)}{E^4} dE, \tag{1}$$

where τ_{D}^0 is the intrinsic lifetime (in the absence of energy transfer) of the donor

emission, R_{DA} is the interaction distance between the ions involved in the transfer, Q_A is the integrated absorbance of the acceptor ion, E is the energy involved in the transfer and $(\epsilon/k^{1/2}\epsilon_c))^4$ is a local field factor. Here ϵ_c is the electric field which would exist at the optically active center if an external field ϵ were to be applied and k is the dielectric constant. Blasse has [25] shown that the term $(\epsilon/k^{1/2}\epsilon_c)^4$ can be put equal to unity without introducing a significant error in the calculations. The factors $F_D(E)$ and $F_A(E)$ represent the normalized shape of the emission band of the donor ion and the absorption band of the acceptor ion, respectively, so that $\int F_D(E)dE = \int F_A(E)dE = 1$. The other symbols in Eq. (1) have their usual meaning. It should be kept in mind that in some special physical situations, the donor ion may be equal to the acceptor ion. Under these circumstances, Eq. (1) relates the probability of donor-donor energy transfer.

By introducing the critical transfer distance R_c, Eq. (1) can be rewritten as follows

$$W_{DA}(DD) = \left(\frac{R_c}{R_{DA}}\right)^6 \frac{1}{\tau_D^0}, \tag{2a}$$

where

$$R_c^6 = \frac{3\hbar^4 c Q_A}{4\pi n^4}\left(\frac{\epsilon}{k^{1/2}\epsilon_c}\right)^4 \int \frac{F_D(E)F_A(E)}{E^4}dE. \tag{2b}$$

The critical distance of energy transfer from the donor ion to the acceptor ion (R_c) is defined as the distance for which the probability of transfer equals the probability of radiative emission of the donor ion, *i.e.*, the distance for which $W_{DA}\tau_D^0 = 1$. Hence, within the lifetime of the donor emission only those acceptor ions within a radius of R_c will be sensitized. The experimental data necessary to calculate R_c are, from Eq. (2b), the integrated absorbance of the optical transition of the acceptor ion and the shape of the emission curve of the donor ion (F_D), and the absorption curve of the acceptor one (F_A). It should be pointed out that R_c is not very sensitive to errors in the calculation of Q_A, F_D and F_A because of the sixth power in Eq. (2b).

Similar expressions can be derived for the transfer of energy by other types of interactions. The transfer rates for the electric dipole-quadrupole (D-Q) and quadrupole-quadrupole (Q-Q) interactions are related to the electric dipole-dipole interaction by

$$W_{DA}(DQ) = \left(\frac{\lambda_D}{R_{DA}}\right)^2 \left(\frac{f_Q}{f_d}\right) W_{DA}(DD), \tag{3}$$

$$W_{DA}(QQ) = \left(\frac{\lambda_D}{R_{DA}}\right)^4 \left(\frac{f_Q}{f_d}\right)^2 W_{DA}(DD), \tag{4}$$

where λ_D is the wavelength of the donor emission transition and f_d and f_Q are

the dipole and quadrupole oscillator strengths of the acceptor transition. Transfer by these higher order multipole processes can be important if electric dipole-dipole transitions are forbidden.

The probability of energy transfer from a donor ion to an acceptor ion by an exchange interaction has also been obtained by Dexter as follows

$$W_{\mathrm{DA}}(\mathrm{exch}) = \frac{2\pi}{h} Z^2 \int F_{\mathrm{D}}(E) F_{\mathrm{A}}(E) dE, \tag{5}$$

where Z is an exchange integral for the donor and acceptor ions. The separation distance is contained in Z and is given by $\exp(-2R/L)$ where L is an "effective average Bohr radius" for the excited and unexcited states of the donor and acceptor ions. Unfortunately, the quantity Z can not be derived from optical measurements. It is important to notice that neither the probability for energy transfer nor the critical interaction distance can be calculated precisely for an exchange interaction mechanism since both quantities are strongly dependent on the wave-function overlap integral of the donor and acceptor electrons involved in the interaction. This makes it important to use accurate expressions for the wavefunctions which are not known at the present time for the most commonly employed optically active impurity ions.

Experimental studies of energy transfer frequently involve an examination of the donor luminescence intensity and lifetime as a function of donor and acceptor concentrations. Observation of the time evolution of the donor luminescence decay following flash excitation provides additional distinguishing features which are helpful in identifying the dominat relaxation mechanisms for energy transfer between donor and acceptor ions.

The decay curve of the donor emission has been discussed theoretically by several researchers [19,23,24] for the case of flash excitation and random distribution of the acceptor ions. Generally, if the energy transfer by resonance takes place from the donor to the acceptor, the decay time τ_{D} of the donor emission becomes smaller in the following manner

$$\frac{1}{\tau} = \frac{1}{\tau_{\mathrm{D}}^0} + W_{\mathrm{DA}}, \tag{6}$$

where τ_{D}^0 is the intrinsic lifetime of the donor ion in the absence of energy transfer and W_{DA} is the rate of energy transfer from the donor to the acceptor ion. The decay curve of the donor emission is still kept to be a single exponential in the case of energy transfer between an isolated pair of donor and acceptor ions. However, in ordinary circumstances the donor is surrounded by a random distribution of acceptors. For such a case, it has been found that the decay curve of the donor emission caused by pulse excitation follows the dependence

$$I(t) = I(0) \exp\left[-t/\tau_{\mathrm{D}}^0 - \frac{4\pi}{3}\Gamma(1 - 3/S) N_a R_{\mathrm{c}}^3 \left(t/\tau_{\mathrm{D}}^0\right)^{3/S}\right], \tag{7}$$

where R_c is the critical transfer distance, N_a is the concentration of the acceptor ions, $\Gamma(x)$ is the gamma function and $S = 6, 8$ or 10 for the case in which the energy transfer takes place by an electric dipole-dipole, dipole-quadrupole or quadrupole-quadrupole interaction mechanisms, respectively. A plot of Eq. (7) reveals that the decay curve of the donor emission is non-exponential, especially in its early part. The non-exponential character of the decay is most evident at short times and for high concentrations of the impurity ions.

If the energy transfer occurs by the exchange interaction, the evolution of the intensity of donor emission is given by

$$I(t) = I_0 \exp\left[-\frac{t}{\tau_D^0} - \frac{\pi}{6} L^3 C_A g\left(\frac{e^{\gamma} t}{\tau_D^0}\right)\right], \tag{8}$$

where $g(Z) = -Z \int_0^l \exp(-Zy)(\ln y)^3 dy$.

In order to obtain Eq. (8), it is assumed that the radial dependence of the interaction is typically described by the expression $(\tau_D^0)^{-1} \exp[\gamma(1 - R/R_c)]$, where $\gamma = 2R_0/L$ and R_c is the critical interaction distance and L has the same meaning as in Eq. (5) *i.e.*, an effective average Bohr radius for the excited and unexcited states of the donor and acceptor ions.

Up to this point, energy transfer from donor to acceptor ions has been discussed on the basis that it occurs without energy migration among the donor system. However, if resonant energy transfer between donor ions is possible, excitation may migrate through the donor system until it comes into the vicinity of an acceptor ion where direct relaxation by donor-acceptor energy transfer can occur. Under these circumstances two regimes are generally considered: (1) diffusion-limited energy transfer from donor to acceptors for somewhat larger donor concentrations, and (2) fast diffusion among donors for very large donor concentrations. In both cases, the transfer rate is dependent on the concentration of the acceptor ions. In the former case, *i.e.* diffusion-limited energy transfer, the time evolution of the donor excitation $\phi(t)$ is found by solving a difussion equation given by

$$\frac{\delta\phi(\mathbf{r}, t)}{\delta t} = D\nabla^2\phi(\mathbf{r}, t) - \sum \nu(\mathbf{r} - \mathbf{r}_n)\phi(\mathbf{r}, t) - \frac{1}{\tau_D^0}\phi(\mathbf{r}, t), \tag{9}$$

where D is the diffusion constant and $\nu(\mathbf{r} - \mathbf{r}_n)$ is the probability for energy transfer from an excited donor to the n^{th} acceptor ion situated at the position $\mathbf{r}_n$. A general solution to Eq. (9) has only been obtained [26] under the assumption that the energy transfer occurs via a dipole-dipole interaction mechanism, and it is given by

$$\phi(t) = \phi(0) e^{-t/\tau_D^0} \exp\left[-\frac{4}{3}\pi^{3/2} N_a (Ct)^{1/2}\left[\frac{1 + 10.87x + 15.50x^2}{1 + 8.743x}\right]^{3/4}\right], \tag{10}$$

where $x = DC^{-1/3}t^{2/3}$ and C is a constant.

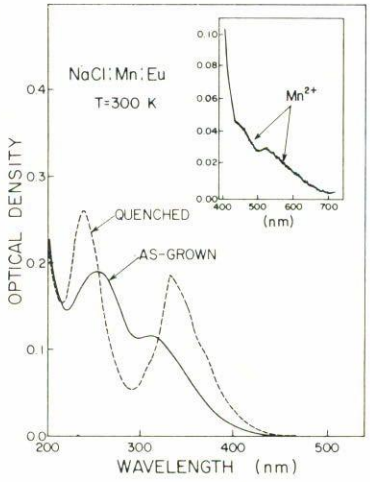

FIGURE 1. Absorption spectra at 300 K for a NaCl:Eu:Mn containing 330 ppm Mn^{2+} and 3 ppm Eu^{2+} in as-grown and quenched samples. The sample thickness was 1.6 cm. The inset displays the weak Mn^{2+} absorption from 400 to 700 nm taken on a 8.3 cm crystal (After Rubio *et al.* 1985).

At earlier times in the donor emission decay, diffusion is unimportant and Eq. (10) reduces to Eq. (7) for $s = 6$, and a non-exponential time dependence is predicted. On the other hand, when $t \to \infty$, Eq. (10) reduces to an exponential function of time with a lifetime approximately given by

$$\frac{1}{\tau} = \frac{1}{\tau_D^0} + \frac{1}{\tau_D}, \tag{11}$$

where $1/\tau_D = 4\pi N_a D\rho$ where ρ is a length defined by $\rho = 0.68(C/D)^{1/4}$.

When the average donor separation is small and the probability for resonant energy transfer between donors is large, then energy diffusion can be very rapidly leading to a spatial equilibrium within the donor system. Under these circumstances variations in the transfer times for different donor-acceptor interaction distances are effectively averaged out and the donor system exhibits a simple exponential decay with a characteristic lifetime value, which decreases when the donor concentration increases.

3. Experimental results

a) The system NaCl:Eu:Mn

The absorption of Eu^{2+} ions in a doubly doped crystal of NaCl containing 330 ppm of Mn^{2+} and 3 ppm of Eu^{2+} is illustrated in Fig. 1 for both as-grown and quenched samples [27]. Although the oscillator strengths in the Eu^{2+} ion transtions

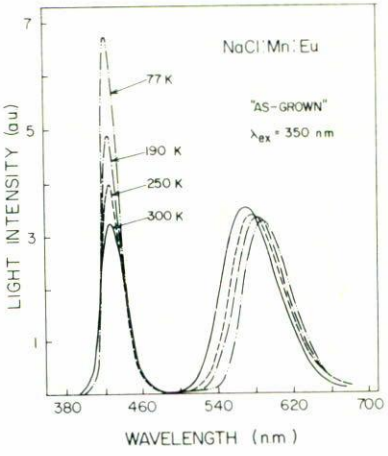

FIGURE 2. Emission spectra for the same crystal used for the data in Fig. 1 as a function of temperature. (After Rubio *et al.* 1985).

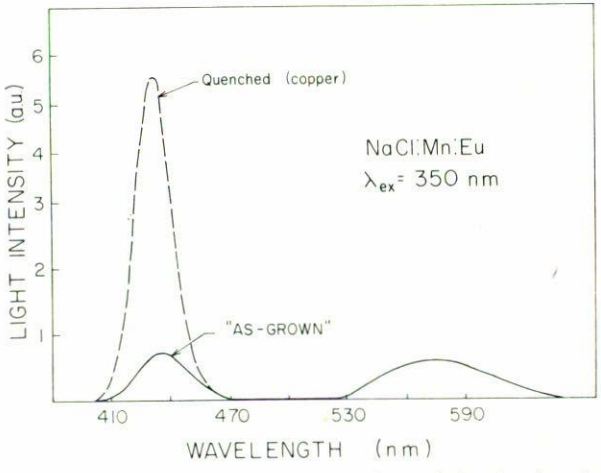

FIGURE 3. Emission spectra at 300 K from the sample used for the data in Fig. 1 as in the as-grown and quenched conditions (After Rubio *et al.* 1985).

is about 10^{-2} and that of Mn^{2+}-ion transitions is only around 10^{-7}, it is possible to detect the Mn^{2+} absorption in relatively thick crystals. When NaCl:Eu:Mn crystals are illuminated with light having the appropriate wavelengths for absorption in the ultraviolet bands, shown in Fig. 1, luminescence is observed. This emission is portrayed in Fig. 2 as a function of temperature. It should be noted that the 580 nm emission peak energy shifts to lower energy (longer wavelength) as the temperature is lowered whereas the 430 nm emission peak energy does not appreciably shift.

Moreover, the area under this latter emission band remains the same for the temperatures measured. Both the peak energy and shift with temperature of the 580 nm band are consistent with Mn^{2+} emission characteristics. At room temperature in the as-grown sample used for Fig. 2 the Eu^{2+} emission and the Mn^{2+} emission have the same peak height intensity. A quench of this sample from high temperature results in an increase in an increase in the 430 nm emission as shown in Fig. 3. However, the 580 nm band remains constant even after rapid quenching in acetone. The same results were found in a crystal containing 100 ppm of Mn^{2+} and 20 ppm and Eu^{2+}, although after quenching a small increase ($\sim$ 15%) in the intensity of the 580 nm band was observed.

When emission from a crystal is observed, it is possible to set the detecting monochromator at the peak energy of the emission, and excite the sample with light from a second monochromator to determine those transitions that contribute to the emission. Since only those transitions which excite luminescence are detected, this is a much more powerful tool than absorption. Fig. 4 shows the liquid-nitrogen excitation spectra for the emission observed at 580 nm. The intense excitation bands are those due to Eu^{2+} transitions, but the weak Mn^{2+} bands can be observed. The room-temperature excitation data for the 430 and 580 nm bands in as-grown and quenched samples is illustrated in Fig. 5. The absorption and excitation data given in Figs. 1, 4 and 5 in conjunction with atomic absorption impurity concentration determination make it possible to derive approximate oscillator strength values for the Eu^{2+} and Mn^{2+} transitions; *i.e.* 2.31×10^{-2} for the Eu absorption and 7.1×10^{-7} for the manganese absorption.

It is evident in Fig. 4 that at low temperatures there is considerable structure present in the excitation bands. From previous research it is well documented that various impurity phases exist in NaCl crystals doped with Mn^{2+} or Eu^{2+} and the absortpion and emission of these impurity phases have been studied in detail [28,29]. The resolution of the data in Figs. 4 and 5 makes it possible to distinguish the transitions of these defects. This will be discussed in more detail later in the paper. For the reader's convenience the transitions energies of the fine-structure bands in the excitation spectra are provided in Tables I and II.

The emission data shown in Fig. 3 indicate that quenching a sample containing much less Eu than Mn results in a marked change in the 430 nm (Eu^{2+}) emission and no measurable change in the 580 nm (Mn^{2+}) emission. If the quenching process produces more Eu^{2+} cation vacancy dipoles this should be evident in the EPR spectra. Fig. 6(a) shows EPR measurements of an as-grown sample, and Fig. 6(b) illustrates the EPR spectrum after the sample has been quenched. It is evident that at least six times as many Eu^{2+} dipoles are detected, but it is also evident that numerous Mn^{2+} dipoles have been produced by the quench even though there is no evidence of an emission increase for the 580 nm band in Fig. 3. At this point, it is important to point out that ITC measurements performed immediately after quenching revealed that not all the Mn ions were completely dispersed into the lattice. For example, for the crystal from which the data shown in Figs. 1–5 were taken, which contained 300 ppm Mn^{2+} ions and 3 ppm Eu^{2+}, only $\sim$ 150 ppm Mn^{2+}-

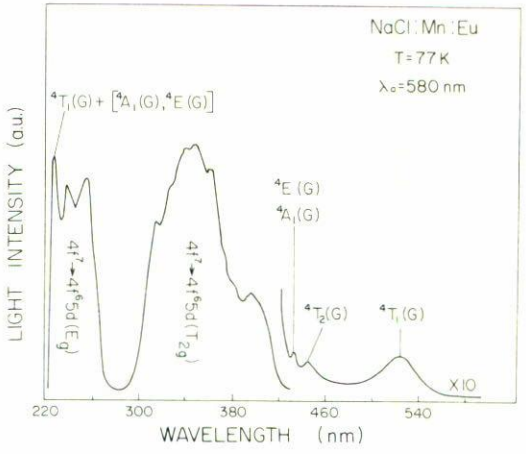

FIGURE 4. Liquid nitrogen excitation spectrum for the orange manganese emission. Assignment of some transitions are also included (After Rubio *et al.* 1985).

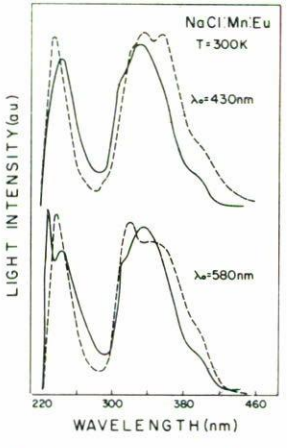

FIGURE 5. Room-temperature excitation spectra for the Mn and Eu emissions in as-grown and quenched samples (After Rubio *et al.* 1985).

cation vacancy dipoles were present after quenching. This fact indicates that Mn aggregates were present in these samples even after a severe quenching in acetone.

The experimental results mentioned above indicate that energy transfer occurs between Eu^{2+} ions and Mn^{2+} ions. This is most easily seen in Fig. 4, where it is apparent that Eu^{2+}-ion absorption produces Mn^{2+} emission. However, the intensity of the Mn^{2+} emission is much greater than can be explained by energy transfer between statistically distributed impurity ions. In fact, for the low Eu^{2+} concentrations

Eu^{2+} state ($4f^6 5d; T_{2g}$)	In isolated Dipoles (nm)	Aggregates (nm)
$^7F_6$	—	317
$^7F_5$	340	332
$^7F_4$	354	345
$^7F_3$	364	354
$^7F_2$	375	368
$^7F_1$	382	382
$^7F_0$	392	397

TABLE I. Positions of Eu^{2+} energy levels in NaCl:Eu at 77 K.

Mn^{2+} state	Suzuki phase		Dipoles	
	Observed (cm^{-1})	Theory[a] (cm^{-1})	Observed (cm^{-1})	Theory[b] (cm^{-1})
$^4T_1(G)$	19011	18870	19380	19100
$^4T_2(G)$	22635	22771	23041	22894
$^4A_1, {}^4E(G)$	24044	23785	23923	23825
		23882		23917
$^4T_2(D)$	27285	27739	27510	27786
$^4E(D)$	28588	28598	28490	28634
$^4T_1(P)$	30257	30329	39395	30148
$^4T_2(F)$	—	37532	—	37696
$^4T_1(F)$	—	40225	—	40145
$^4T_2(F)$	—	41337	—	41184
$^4T_1(G) + [^4E(G), {}^4A_1(G)]$	43478			

[a] Obtained using $Dq = 625$ cm^{-1}, $B' = 840$ cm^{-1}, and $\epsilon = 0.038$.
[b] Obtained using $Dq = 600$ cm^{-1}, $B' = 838$ cm^{-1}, and $\epsilon = 0.034$.

TABLE II. Positions of Mn^{2+} energy levels in the doubly doped samples at 77 K.

in these smaples no effects of energy transfer would be observed if the impurity ions were distributed statistically.

The fact that energy transfer is observed in the samples implies that the impurities are not randomly distributed but rather occur as coupled pairs of Eu^{2+}-Mn^{2+}. This pairing might be expected in NaCl since Eu^{2+} has an ionic radius of 1.12 Åand Mn^{2+} an ionic radius of 0.8 Å. If these two ions couple through a Cl ion along a ⟨100⟩ direction, then they must fit into a space of 5.6 Å. Since Mn^{2+} is smaller than Na^+ (R = 0.98 Å) and Eu^{2+} is larger, the two ions together fit perfectly in the allowed space in the lattice of sodium chloride.

The change in absorption due to quenching can be explained as due to Mn-ion clusters around the Eu-Mn pairs being dispersed by the quenching procedure. If this occurs, a small shift of the Mn^{2+} emission should be observed after quenching. Such an effect was found. In fact, low-temperature high-resolution data show that Mn^{2+} emission is slightly red-shifted after quench. The dispersion of Mn^{2+} clusters is also evidenced by the increased Mn^{2+}-dipole concentration immediately after quenching (Fig. 6).

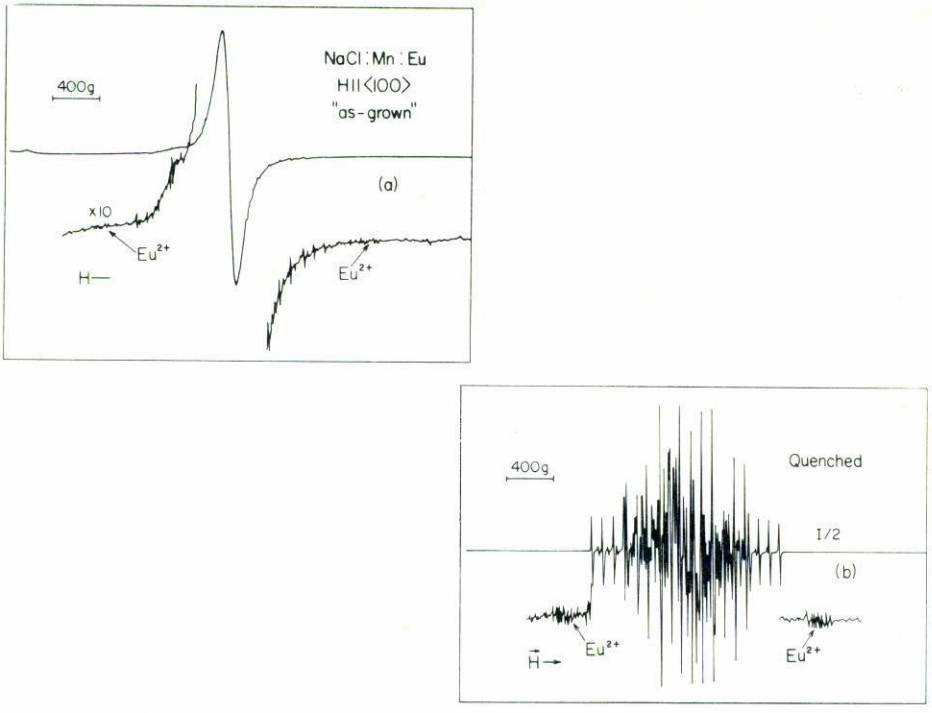

FIGURE 6. Electron paramagnetic resonance spectra at 300 K for the same used for the preceding figures: (a) before quenching, (b) after quenching. In this figure sample the letter I represents the amplifier gain used to record the spectra (After Rubio *et al.* 1985).

The fact that the fluorescence lifetime of the Eu^{2+} emission ($\sim 1\mu s$) in the quenched sample is not decreased by the presence of the Mn^{2+} can be explained by assuming that all of the observed Eu^{2+} fluorescence under these conditions originates from ions not paired with a Mn^{2+} ion, whereas all of the paired Eu^{2+} ions transfer their energy so efficiently that they make no contribution to the observed fluorescence. The non-exponential decay pattern with a shortened lifetime for Eu^{2+} in the as-grown NaCl:Eu,Mn sample implies that the small number of Eu^{2+} ions which are not directly paired with Mn^{2+} ions are distributed at varying close separations from Mn^{2+} ions. One possibility for explaining this type of distribution is the presence of Eu^{2+} ions within a Suzuki-phase region of Mn^{2+} ions [29]. These regions are known to be present in about 10% of the as-grown crystal volume. The quenching treatment breaks up 90% of these regions as well as other impurity aggregates, and the observed Eu^{2+} emission is dominated by ions too far away from any Mn^{2+} ion to interact through energy transfer.

Previous work has illustrated the propensity for precipitates [29,30,31] and Suzuki phases [32–37] in this material. These defects and their effects can be seen in the data presented above. Since precipitates, or even the Suzuki phase, take up only

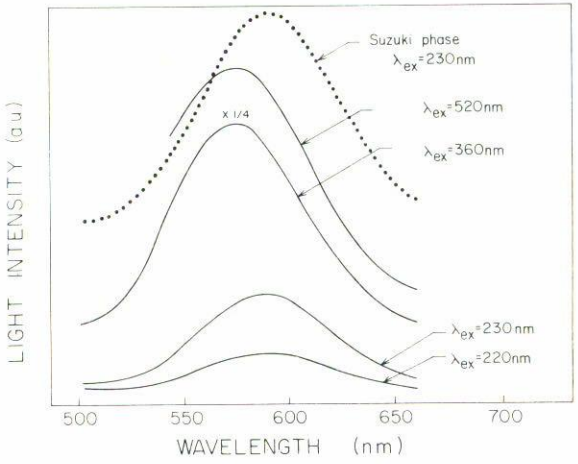

FIGURE 7. Manganese emission spectra for various wavelengths of exciting light at 300 K in as-grown samples of NaCl:Eu:Mn. In the same figure, the emission spectrum of a NaCl:Mn sample in which the impurity is precipitated into the Suzuki phase is shown for comparison (After Rubio *et al.* 1985).

a small volume of the crystal the effects are small, but nonetheless observable. Fig. 7 shows the emission for Mn^{2+} ions in the Suzuki phase ($\lambda_{ex} = 230$ nm) with no Eu^{2+} ions in the crystal (dashed line) and from Mn^{2+} ions in the doubly doped samples through direct excitation ($\lambda_{ex} = 520$ nm). The intensity of the Mn^{2+} emission and the energy of this emission peak when excited with $\lambda_{ex} = 360$ nm indicates energy transfer from Eu^{2+} to Mn^{2+}. The presence of a band similar to the Suzuki-phase Mn^{2+} emission in these NaCl:Eu,Mn crytals suggests that the Suzuki phase of the Mn^{2+} ions has been nucleated in the latter as-grown samples.

The structure appearing in the spectra can be explained through crystal-field considerations. The excitation spectra of the Mn-emission band taken in the as-grown samples and for a sample temperature in the range (12–77 K) show a complex structure due to the superposition of the Eu^{2+} and Mn^{2+} absorption transitions. As has been previously mentioned, in the as-grown samples there are several types of Eu-Mn and Mn-Mn defect complexes. In the case of Eu-Mn pairs, it is expected that the crystal field acting on the europium ion should be mainly that of O_h symmetry as in the case of isolated Eu^{2+} ions, since the presence of a neighboring Mn^{2+} ion constitutes only a small perturbation to this crystal field. This can be verified by comparing the observed spectral structure obtained from the excitation spectra of NaCl:Eu with the number of transitions to ^7F_j levels predicted in O_h symmetry, as listed in Table I. On the other hand, the orthorhombic crystal field due to the ⟨110⟩ charge compensating vacancy gives rise to a small crystal-field splitting of each J multiplet as has been discussed elsewhere [38]. The doubly doped samples present slightly broader transitions indicating that the interaction with the Mn^{2+} gives rise to a small perturbation only. Table I also lists the excitation peaks that appear in

the low-energy band (T_{2g}) of the Eu^{2+} spectra for small aggregates. These peaks correlate quite well with some of those appearing in the doubly doped samples, which may then be due to an aggregate of Mn^{2+} ions in which the Eu-Mn pair has acted as a nucleation center.

The other peaks appearing in the excitation spectra of the doubly doped as-grown samples are due to Mn^{2+} ions precipitated in the Suzuki phase. The presence of this second-phase precipitate was established through the observation of the 230 nm band in the excitation spectra of the Mn^{2+} emission and ascribed to a double quantum transition ${}^6A_1 \rightarrow {}^4T_1(G) + [{}^4A_1(G), {}^4E(G)]$ as has been discussed by Rodríguez *et al.* [29].

In quenched crystals the overlap of the Eu^{2+} bands with those of the Mn^{2+} ions makes it difficult to measure precisely the Mn^{2+} peak positions. However, within experimental error, the measured peak positions in the doubly doped samples coincide with those reported by Rodríguez *et al.* [29] and are also similar to the as-grown case.

The Mn^{2+} crystal-field transitions were fit using the procedure developed by Curie *et al.* [39] instead of the usual procedure of treating the Racah parameters B and C and the crystal-field splitting $10Dq$ as adjustable fitting parameters. The latter authors have shown that the inclusion of covalent effects, as well as the Racah-Tress and seniority corrections, provide better fits to Mn^{2+} data. In this procedure the adjustable parameters are Dq, a covalent reduced Racah parameter $B'(= BN_\tau^4)$, and the Koide-Pryce [40] covalency parameter ϵ. The results obtained using this procedure are shown in Table II for both Mn^{2+} ions in the dipolar state and the Suzuki phase. It should be noted that the effective $10Dq$ values found here [27] are different from those obtained by Rodríguez *et al.* [29]. This is due to the fact that Rodríguez *et al.* used the Racah-Trees and seniority corrections in the weak-field scheme, whereas the energy-level structure of the Mn^{2+} ion was derived from the matrices obtained from the strong-field scheme in which these corrections are not diagonal. Using a similarity transformation, we have obtained the energy matrices in the strong-field scheme, including the corrections mentioned above, following the procedure employed by Mehra [41]. The Racah-Trees and seniority corrections are specified by the parameters α and β, respectively, whose values were taken as in the free-ion case following Curie *et al.* [39]. ($\alpha = 65$ cm^{-1} and $\beta = -131$ cm^{-1}). The values obtained for B' and ϵ for Mn^{2+} into the Suzuki phase are quite similar to those obtained by Curie *et al* for $MnCl_2 \cdot 2H_2O$ ($B' = 0.911$ and $\epsilon = 0.024$). This result may suggest that in the Suzuki phase of the Mn^{2+} ions in the NaCl lattice, the Mn^{2+}-Cl^- distance is around 2.7 Å.

Europium-manganese pair formation in the lattice of NaCl has been recently analyzed by Muñoz and Rubio [42] as a function of various cooling rates as well as of the room temperature annealing of the doubly doped crystals. To do this, photoluminescence, pulse excitation, and electron paramagnetic resonance measurements were carried out in parallel. The crystals employed contained very low concentrations of the donor and acceptor ions in order to clearly demonstrate impurity pair formation in the alkali halide matrix even after an efficient quench into acetone.

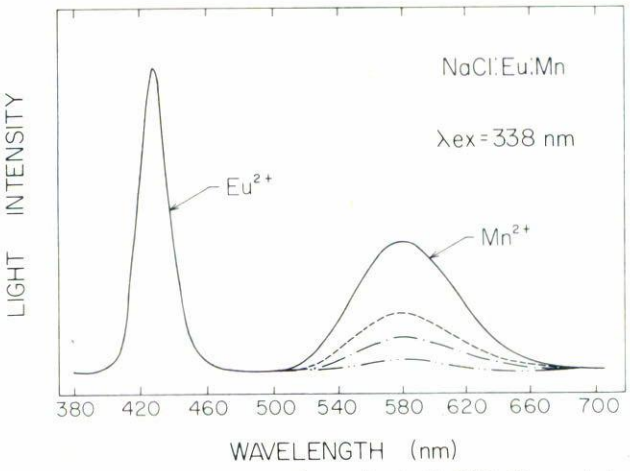

FIGURE 8. Liquid nitrogen emission spectra of several twin NaCl:Eu:Mn crystals after they were heated for 1 h at 873 K and then cooled in natural air (—), quenched onto a massive copper block (- - -), into liquid nitrogen or alcohol (- · -), and into acetone (- · · -). (After Muñoz and Rubio 1989).

In Fig. 8 we show the room temperature emission spectra of several NaCl:Eu:Mn twin samples after they were heated for one hour at 873 K and then cooled to room temperature using various methods of cooling: such as natural cooling in air, placing onto a massive copper block, quenching into alcohol, into liquid nitrogen, and into acetone. All of these, apart from the acetone quench are relatively slow quenches as revealed by the work of Taylor *et al.* [43]. To obtain this information the spectra were taken within 3 min after the quenching treatment on samples with dimensiones of $0.4 \times 0.4 \times 0.01$ cm^3. The spectra shown in this figure consist of two broad bands in the blue (428 nm) and in the orange-red (580 nm) regions of the electromagnetic spectrum. The former band is due to the de-excitation of the Eu^{2+} ions from the excited state $4f^6 5d(E_g)$ to the ground state $^8S_{7/2}$. The orange-red band appears only after the NaCl:Eu crystals are simultaneously contaminated with doubly valent manganese ions and it is attributed to the transition $^4T_1(G) \rightarrow {}^6A_1$ of these ions.

Reference to Fig. 8 shows that the ratio of the intensities (I_{Mn}/I_{Eu}) of the manganese and europium emission bands is critically dependent on the cooling procedure employed and increases with the use of the less efficient quenches.

The liquid nitrogen excitation spectra of the Eu^{2+} and Mn^{2+} emissions taken immediately after a doubly doped crystal was quenched into acetone are portrayed in Fig. 9. In both cases, the spectrum consists of the two broad absorption bands typical of the Eu^{2+} ions. They are associated with the dipole allowed $4f^7 \rightarrow 4f^6 5d(E_g : T_{2g})$ transitions [38]. The separation between these two bands is a measure of the $10Dq$ splitting of the $5d$ orbital into its E_g and T_{2g} components due to the crystal field acting at the europium site. Manganese emission is, therefore, produced by exciting into either the high and low-energy absorption bands of the Eu^{2+} ions. This

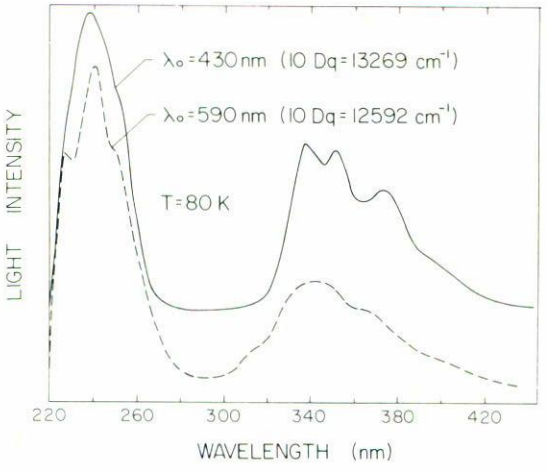

FIGURE 9. Liquid nitrogen excitation spectra for the Eu^{2+} and Mn^{2+} emission bands taken immediately after the doubly doped NaCl crystal was quenched into acetone. Values for the $10Dq$ splitting measured from each spectrum are given. (After Muñoz and Rubio 1989).

fact clearly demonstrates that Eu→Mn energy transfer occurs in the NaCl crystals doubly doped with europium and manganese ions in agreement with the previous observations mentioned above.

It was ascertained that the europium emission peaking at 428 nm decreases to the benefit of the Mn^{2+} emission peaking at 580 nm as the time elapsed at room temperature between quench and measurement increased. The detailed kinetics for both emission bands is given in Fig. 10 for a crystal which was previously quenched into acetone. It is observed from these data that the intensity of the Eu^{2+} emission decays $\sim$ 30% after 2 hours of room temperature aging. This decay is well correlated with the growth in intensity of the manganese emission. For longer annealing times, the rate of intensity decay of the Eu^{2+} fluorescence and the rate of growth of the manganese emission slow down and almost a plateau is observed for times up to $\sim$ 2000 h. Similar results were obtained in the samples which were quenched onto a massive copper block, into alcohol, or into liquid nitrogen, although the rate of intensity decay of the Eu^{2+} emission and the rate of growth of the Mn^{2+} emission were found to be faster.

In order to get additional information of the processes taking place during the room temperature annealing of the acetone quenched crystals, EPR measurements were also carried out in parallel with the optical ones. The evolution of the EPR signal intensity associated with the Eu^{2+} and Mn^{2+}-cation vacancy dipoles still in solution in the crystal is portrayed in Fig. 11 as a function of the aging time at 300 K. In the same figure, the evolution of the intensity of the Eu^{2+} fluorescence is also given for comparison purposes. In order to obtain the EPR data, the intensities of the lowest field hyperfine lines in both the Eu^{2+} and Mn^{2+} dipolar spectra, when

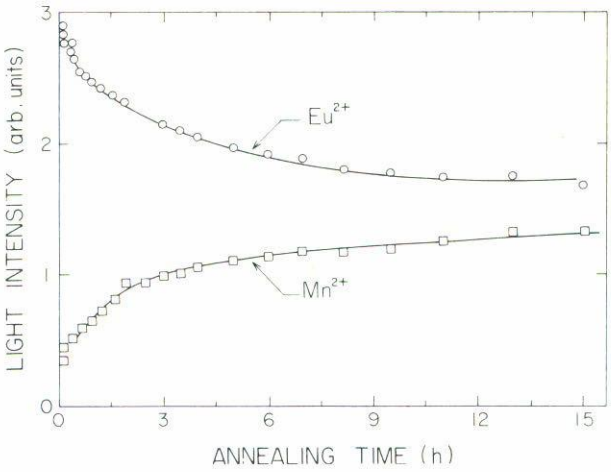

FIGURE 10. Evolution of the intensities of the Eu^{2+} and Mn^{2+} emissions observed in an acetone quenched crystal of NaCl as a function of the annealing time at 300 K. The intensity of the manganese emission was multiplied by a factor of 4. (After Muñoz and Rubio 1989).

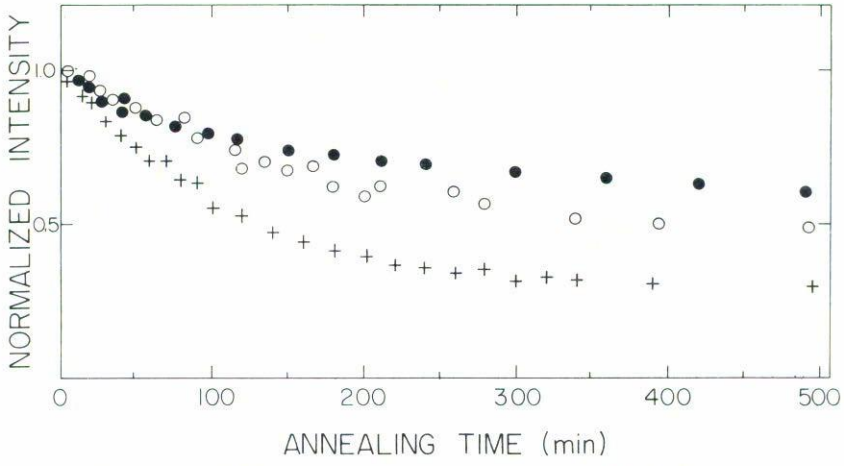

FIGURE 11. Decay of the EPR signal intensities associated with the Eu^{2+}-cation vacancy dipoles (0) and Mn^{2+}-cation vacancy dipoles (+) as a function of the aging time at 300 K in a NaCl crystal which was heated for 1 h at 873 K and then quenched into acetone. In the same figure the evolution of the Eu^{2+} emission intensity (0) is also portrayed for comparison purposes (After Muñoz and Rubio 1989).

the magnetic field was applied along the [001] direction, were measured as a function of the time elapsed between quench and measurement.

Pulse excitation measurements performed immediately after the crystals were quenched into acetone revealed that the decay of the Eu^{2+} fluorescence consisted

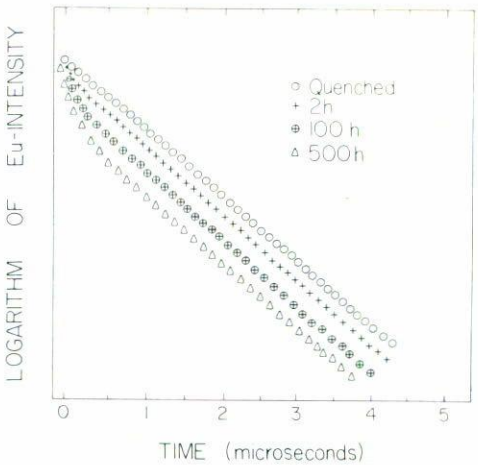

FIGURE 12. Semilogarithmic plots of the Eu luminescence decay taken at different times during the room temperature annealing of previously acetone quenched crystals of NaCl (After Muñoz and Rubio 1989).

of a pure exponential decay with an associated lifetime value of $1\mu s$, unlike the non-exponential decays usually observed when donor-acceptor energy transfer takes place. The same overall luminescence decay was found to occur for times up to ~ 2 h during the room temperature annealing. At longer annealing times, however, the Eu^{2+}luminescence decay was characterized by an initial non-exponential portion followed by the intrinsic lifetime value ($1\mu s$); the amplitude of the non-exponential portion being larger as the time elapsed between quench and measurement increased. Examples of such luminescence time dependences are illustrated in Fig. 12, where semilogarithmic plots of the Eu^{2+} fluorescence decay for different annealing times at room temperature are shown.

At this point, it is important to emphasize that the decay scheme of the Eu^{2+} luminescence decay observed in the doubly doped samples immediately after they were quenched into acetone was the same as the one found in NaCl contaminated with a small concentration of Eu^{2+} ions. This decay is characterized by a pure exponential decay with a lifetime value of $1\mu s$.

On the other hand, the decay scheme of the manganese ions was characterized by a pure exponential decay with a time constant of 28 ms for times up to ~ 100 h. At longer annealing times, however, the luminescence decay became complex and non-exponential decays were predominantly observed.

The overall decay scheme of the Eu^{2+} and Mn^{2+} emissions in the doubly doped samples which were quenched into alcohol, into liquid nitrogen or onto a massive copper block were found to be nearly identical to those determined in the acetone quenched crystals. Immediately after the quench, the Eu^{2+} and Mn^{2+} luminescence decays were single exponential with lifetime values of $1\mu s$ and 28 ms, respectively. However, the growth of the non-exponential portion at short times in the decay of

the Eu^{2+} luminescence, as well as, the appearance of the non-exponential decays for the Mn^{2+} emission, occurred at shorter times during the room temperature annealing.

On the other hand, the decay scheme of the Eu fluorescence in the doubly doped samples which were unefficiently quenched in natural air consisted, immediately after the quench, of a clearly observable non-exponential portion at short times in the decay followed by the intrinsic decay rate. The manganese luminescence decay was found to be similar than the one determined in the acetone quenched crystals.

The importance of rapid cooling from high temperatures to retain a random dispersion of impurities in alkali halide crystals doped with doubly valent impurity ions (M^{2+}) has been discussed by Taylor *et al.* [43]. These authors found that one may prevent and obtain virtually all the M^{2+} ions isolated at room temperature if sufficiently rapid quenches and low impurity concentrations are employed. Moreover, very thin crystals with relatively small broad face areas should be used. Otherwise, substantial clustering and even precipitation can occur in crystals which contain as little as 40 ppm of divalent cations during the quenching procedure.

According to these authors the acetone quench is capable of giving a fully efficient quench if the thickness of the crystal is ~ 0.5 mm. Quenching onto a copper block, into mineral oil, into liquid nitrogen or in natural air, however, may not give a fast enough quench to prevent impurity clustering.

The data portrayed in Fig. 8 show that even after an efficient quench into acetone, energy transfer from europium to manganese ions takes place in the slightly doubly doped samples. For the low concentrations of the donor and acceptor ions in the crystals employed, it is not possible that the observed Eu-Mn energy transfer would take place between the impurities randomly distributed in the lattice. In fact, if we assume this situation, the rate of Eu→Mn energy transfer calculated from the use of either an electric dipole-dipole or a dipole-quadrupole interaction mechanism is found to be quite small compared with the intrinsic radiative decay rate of the isolated Eu^{2+} ions. Therefore, one may conclude that the Eu→Mn energy transfer which is observed in the acetone quenched crystals occurred in the Eu-Mn pairs which were preferentially formed in the lattice of NaCl.

The excitation spectra shown in Fig. 9 for the Eu^{2+} and Mn^{2+} emissions which were taken immediately after the samples were quenched into acetone, reveal that the magnitude of the $10Dq$ splitting of the $5d$ orbital into its E_g and T_{2g} components, calculated from the excitation spectrum of the Eu-emission (13,269 cm^{-1}) is larger than that determined from the excitation spectrum of the Mn^{2+} emission (12,592 cm^{-1}). This result indicates that the crystal field acting at the site occupied by the Eu^{2+} ion when it is forming isolated Eu^{2+}-cation vacancy dipoles in the lattice of NaCl is larger than the acting at the site occupied by the europium ion when it is coupled to a manganese ion. This finding supports the original idea of Rubio *et al.* [27] in the sense that europium-manganese pair formation is favored in the lattice of NaCl in order to reduce the strain in the lattice induced by the presence of each impurity alone.

However, pair information is enhanced when the crystals were stored at room temperature after the quench. The data portrayed in Fig. 11 clearly show that

the decay of the EPR signal intensity due to isolated Eu^{2+}-cation vacancy dipoles correlates quite well with the decay of the Eu^{2+} luminescence for annealing times up to $\sim$ 2 h. At longer annealing times, the EPR intensity of the Eu^{2+} dipolar complexes decays faster than that of the Eu^{2+} fluorescence. This behaviour can be correlated with the pulse excitation measurements performed at different times during the storage of the specimens at room temperature. These measurements show that the decay scheme of the Eu fluorescence consisted of a pure exponential decay with an associated lifetime value of 1μs for annealing times up to $\sim$ 2 h. At longer annealing times an initial non-exponential portion followed by the intrinsic decay was observed for times up to $\sim$ 2000 h; the amplitude of the non-exponential portion was found to be larger as the time elapsed between quench and measurement increased.

All these data together may be explained considering that isolated Eu^{2+} and Mn^{2+} cation vacancy dipoles, as well as Eu-Mn pairs are mainly the complexes which exist in the samples after they are efficiently quenched into acetone. On the other hand, the pairs are the types of aggregate complexes which are mainly formed during the room temperature annealing for times up to 2 h after the quenching treatment. Due to this pair formation the intensities of the Eu^{2+} fluorescence and of the EPR spectrum associated with the Eu^{2+} dipolar complexes still in solution, decay as a function of the aging time, in a correlated way with the growth in intensity of the manganese emission.

When the Eu-Mn pair is formed, the $Eu^{2+} \rightarrow Mn^{2+}$ energy transfer which takes place in the complex is so efficient that quenches the sensitizer emission completely. Therefore, the Eu^{2+} luminescence observed in the doubly doped samples after they are quenched into acetone or annealed at room temperature for times up to $\sim$ 2 h is due to those europium ions forming dipolar complexes which are not interacting with any manganese ions. Under these circumstances the overall decay scheme of the Eu^{2+} fluorescence in quenched or slightly annealed NaCl:Eu:Mn crystals should be the same as that in NaCl slightly contaminated with europium ions. This expectation is confirmed by the experimentally determined data presented above.

As the annealing time proceeds the pairs may act as efficient nucleation centers for the manganese ions, inducing therefore, the formation of large manganese aggregates and even second phase precipitates in which some europium ions are embedded. In these more complex aggregates or precipitates a larger fraction of the excited Eu^{2+} ions are within the effective interaction sphere of the Mn^{2+} energy sinks, and a non-exponential portion at short times in the Eu fluorescence decay is expected due to different europium-manganese interaction distances; the non-exponential portion being more prominent in the overall decay as the time elapsed at room temperature between quench and measurement increased due to the growth of the impurity aggregates. In these aggregates (precipitates) a single pair donor-acceptor energy transfer mechanism is active [44]. It can not be ignored, however, that manganese aggregates and even second phase precipitates without any incorporated europium ions may be formed during the room temperature aging.

The pure exponential decay of the manganese emission characterized by a lifetime value of 28 ms may be associated with those manganese ions which were

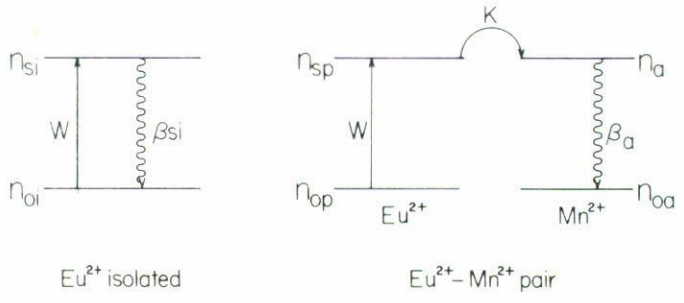

FIGURE 13. Energy level system used to describe the essential features of the kinetics of Eu→Mn energy transfer in NaCl (After Muñoz and Rubio 1989).

paired or forming small aggregates in the doubly doped crystals. For annealing times larger than $\sim$ 100 h the decay became non-exponential suggesting the formation of different types of aggregates. In each one of these aggregates, the decay scheme of the manganese emission appears to be different.

Finally, the number of Eu-Mn pairs present in the crystals after they were quenched using various methods of cooling can be estimated using the model depicted in Fig. 13. In this model [42,45] both the europium and manganese ions are treated as two energy-level systems and the experimental observations mentioned above have been incorporated.

The rate equations describing the time evolution of the excited state populations of both isolated europium ions and Eu-Mn pairs are given by

$$\begin{aligned} \frac{dn_{si}}{dt} &= Wn_{oi} - \beta_{si}n_{si}, \\ \frac{dn_{sp}}{dt} &= Wn_{op} - Kn_{sp}, \\ \frac{dn_o}{dt} &= Kn_{sp} - \beta_o n_o, \end{aligned} \tag{12}$$

where n_{si} and n_{sp} are the populations of the excited states of the Eu ion when it is isolated and in the coupled form respectively, n_{oi} and n_{op} are the corresponding populations for the ground state, n_o is the concentration of the excited state of the manganese ions forming the impurity pairs, β_{si} and β_o are the fluorescence decay rates of the isolated europium and coupled manganese ions, K is the rate of energy transfer and W is the absorption probability which has been assumed to be the same for both isolated and coupled europium ions. Direct excitation of Mn^{2+} has been

considered to be negligible in view of the forbidden nature of the $d \rightarrow d$ absorption transitions.

We can easily solve Eqs. (12) for continuous excitation to give the ratio for the number of europium ions which are paired with the manganese ions (N_{sp}) and the total concentration of europium ($N_{st} = N_{si} + N_{sp}$) in the crystals

$$\frac{N_{sp}}{N_{st}} = \frac{I_a(\beta^r_{si}/\beta_{si})}{I_{si}\left[\beta^r_a/\beta_a + \left(\frac{I_a}{I_{si}}\right)\frac{\beta^r_{si}}{\beta_{si}}\right]}; \tag{13}$$

where the β^r are the radiative decay rates of the levels, and I_{si} and I_a are the integrated intensities of the europium and manganese emissions observed in the doubly doped crystals immediately after the quench.

Considering that the radiative decay rates are equal to the inverse of the low temperature (11 K) lifetime values ($\beta^r_{si} = 1\times10^6 S^{-1}$; $\beta^r_a = 22S^{-1}$), N_{sp}/N_{st} is found to be ~ 0.13 when the experimentally determined room temperature data obtained in the acetone quenched crystals are employed in Eq. (12) (*i.e.* $\beta_{si} = 10^6 S^{-1}$; $\beta_a = 36S^{-1}$ and $I_a/I_{si} \cong 0.10$). Thus, about 13% of the total concentration of the Eu^{2+} ions in the doubly doped crystals of NaCl are paired with the manganese ions even after the samples are efficiently quenched into acetone. This percentage is larger when the slower cooling rates, such as those characterized by quenching into liquid nitrogen (or alcohol) ($\sim$ 17%) or onto a massive copper block ($\sim$ 25%), are employed in view of the enhanced probability for impurity pair formation.

At this point, it is important to note that the ratio I_a/I_{si} is larger when the doubly doped samples were inefficiently quenched in natural air. However, the lifetime measurements indicate that the Eu→Mn energy transfer which is observed in this type of crystals does not only occur in the Eu-Mn pairs but also in some small europium-manganese aggregates which were formed during the quenching procedure. Therefore, an estimation of the number of pairs in this case is not possible in view of the lack of information of the number of europium ions transferring their energy to the manganese ions in the aggregates.

Let us now discuss the possible mechanism for the $Eu^{2+} \rightarrow Mn^{2+}$ energy transfer taking place in the samples of NaCl [46]. Taking into account that the isolated pair transfer rate is time independent, solutions to the rate Eq. (12) can be obtained under the assumption that W represents a delta function excitation pulse

$$n_s(t) = n_s(0)\exp[-\beta_{sit}],$$

$$n_a(t) = \frac{+Kn_s(0)}{(\beta_a - k)}(\exp[-Kt] - \exp[-\beta_a t]). \tag{14}$$

The time at which the activator fluorescence intensity reaches it maximum value (t_{max}) can be found by setting the first time derivative of $n_a(t)$ equal to zero. This

gives

$$t_{max} = \frac{1}{(K - \beta_a)} \ln(K/\beta_a). \tag{15}$$

When the value for $t_{max} < 25$ ns and the experimentally determined decay time of the manganese emission in the slightly-doped crystals are employed in Eq. (15), the rate of $Eu^{2+} \rightarrow Mn^{2+}$ energy transfer is found to be $> 5 \times 10^8 S^{-1}$ at 300 K.

The forbidden nature of the $3d \rightarrow 3d$ Mn^{2+} absorption transitions suggests that the $Eu^{2+} \rightarrow Mn^{2+}$ energy transfer mechanism which takes place between these two impurity ions is either of the electric dipole-quadrupole type or exchange in nature. According to Dexter's theory of energy transfer, the transfer rate for an electric dipole-quadrupole interaction mechanism is given by

$$W_{DA}^{DQ} = \frac{3h^4c^4Q_a}{4\pi n^4\tau_D^0} \frac{f_Q}{f_d} \frac{(\lambda_s)^2}{(R_{DA})^8} \int \frac{F_D(E)F_A(E)}{E^4} dE, \tag{16}$$

where the symbols employed have been explained in Eqs. (1–4). Since the absorption coefficient of manganese is quite difficult to measure, Q_a was estimated using the expression derived by Blasse *i.e.* [25], $Q_a = 4.8 \times 10^{-16} f_d$ where $f_d \cong 10^{-7}$ for Mn^{2+} ions. To obtain $F_A(E)$ we employed the absorption spectrum of Mn^{2+} in NaCl given by Rodríguez *et al.* [29]. This was done since we were not able to obtain the absorption spectrum of the manganese ion in the overlap region of the Eu^{2+} emission because of its small concentration. Moreover, this spectrum has not been reported in the literature, as far as we know. This approximation is, however, a reasonable one since the absorption spectra of Mn^{2+} in several alkali halides are very similar, as has been shown by Rodríguez *et al.* The normalized line-shape functions for the Eu-emission and the Mn-absorption in the overlap region are shown in Fig. 14. With this approximation the value of Ω was found to be 3.39×10^{-2} eV^{-5}.

Since the exact nature of the Eu-Mn pair complex can not be inferred from our experimentally determined data, the rate of energy transfer via a dipole-quadrupole interaction mechanism was calculated using different configurations for the Eu-Mn dimer, such as those given in Fig. 15. Defect and binding energies for these types of dimers have been calculated for different kinds of doubly valent impurity ions in the alkali halides by Bannon *et al.* The obtained values for W_{DA}^{DQ} for each of the considered dimer complexes are given in Table III. In the same table, the rate of energy transfer calculated from the use of an electric dipole-dipole interaction mechanism is also included for the sake of comparison. The closer agreement between the calculated values for W_{DA}^{DQ} and that estimated experimentally is achieved when the ⟨100⟩ dimer configuration (D_1) is employed to perform the calculations. The calculated value appears, however, smaller than that estimated from the experimentally determined data. This fact may suggest that an exchange (superexchange) interaction mechanism is probably the responsible for the energy transfer from the europium to the manganese ions in the lattice of NaCl. Such interaction can lead to energy transfer rates much higher than those predicted from Eq. (16). In fact,

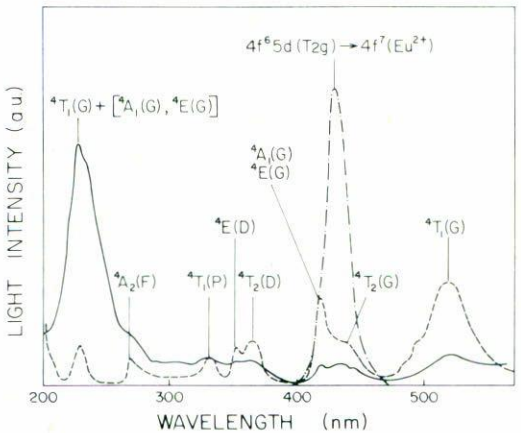

FIGURE 14. Overlap region of Eu^{2+} emission and Mn^{2+} absorption in NaCl at 300 K. The latter spectrum was taken from Rodríguez *et al.* (Ref. [29]).

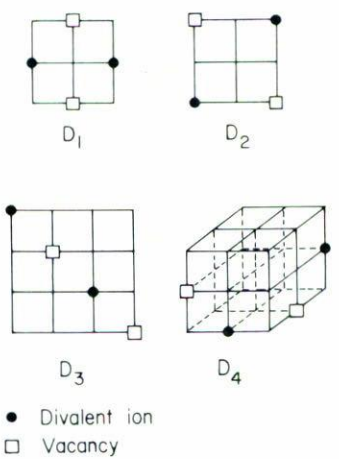

FIGURE 15. Possible configurations for the Eu-Mn dimer complex in the lattice of NaCl which were considered to calculate the rate of energy transfer via multipolar or exchange interaction mechanisms.

magnetic studies [48] have shown that exchange between cations can be relatively strong for 180° interactions involving one *p*-orbital of an anion intermediary, as it is the case in the D_1 dimer configuration.

Unfortunately, only a very rough estimation for the rate of energy transfer using a superexchange interaction mechanism is possible at the present time. The reason for this fact is that the wavefunction overlap integral of the sensitizer and

System	Configuration	Distance R_{DA}(A)	W_{DA}(DD) S^{-1}	W_{DA}(DQ) S^{-1}
NaCl:Eu:Mn	D_1	5.6	3.16×10^5	1.87×10^8
	D_2, D_3	7.9	3.95×10^4	1.17×10^7
	D_4	6.8	9.35×10^4	3.70×10^7
NaBr:Eu:Mn	D_1	5.9	0.30×10^6	1.60×10^8
	D_2, D_3	8.3	3.70×10^4	1.00×10^7
	D_4	7.2	8.90×10^4	3.15×10^7
NaI:Eu:Mn	D_1	6.5	8.6×10^4	4.0×10^7
	D_2, D_3	9.1	1.1×10^4	2.5×10^6
	D_4	7.9	2.6×10^4	7.9×10^6
KCl:Eu:Mn	D_1	6.3	1.56×10^5	0.70×10^8
	D_2,D_3	8.9	1.96×10^4	4.88×10^6
	D_4	7.7	4.68×10^4	1.39×10^7
NaCl:Sn:Mn	D_1	5.6	7.98×10^4	0.50×10^8
	D_2, D_3	7.9	9.99×10^3	3.14×10^6
	D_4	6.8	2.36×10^4	9.87×10^6

TABLE III. Calculated rates of Eu→Mn and Sn→Mn energy transfer in different host crystals using Dipole-Dipole (DD) and Dipole-Quadrupole (DQ) interaction mechanisms.

activator electrons involved in the interaction can not be calculated since accurate expressions for the wave functions are not known. The estimation can be obtained from the expression derived by Dornauf and Heber [49] for the transfer probability in the case of superexchange

$$W_{DA}(\text{exch}) = \frac{1}{\tau_D^0} \exp[\gamma(R_c - R_{DA})], \tag{17}$$

where τ_D^0 and R_{DA} have the same meaning as above, R_c is the critical interaction distance and γ is the exchange constant, which according to Dexter is equal to $2/L$ where L is an "effective average Bohr radius" for the excited and unexcited states of the paired complex. Using the D_1 dimer configuration, a value for R_c similar to that found for the dipole-quadrupole interaction mechanism (~ 10Å) and a typical value for the "effective Bohr radius" of ~ 1.05Å which is about half of the manganese-chlorine separation, a rate of $4.3 \times 10^9 S^{-1}$ is obtained. If we juxtapose this result to the W_{DA}(DQ) calculated above, we may conclude that Eu→Mn energy transfer via a superexchange interaction mechanism appears to have a higher probability than Eu→Mn energy transfer via a multipolar interaction mechanism. On the other hand, the large distances between donor and acceptor ions, as well as their locations in the other types of dimer complexes such as those given in Fig. 15, appear to be less appropriate for the occurrence of this type of interaction.

Although, it is recognized that these calculations are phenomenological they may suggest that the possible nature of the Eu-Mn complex could be that of the D_1 dimer. They also indicate that the experimentally determined data can only be explained if a short range interaction mechanism such as an electric dipole-quadrupole or exchange in nature is active between the europium and manganese ions forming the impurity pairs.

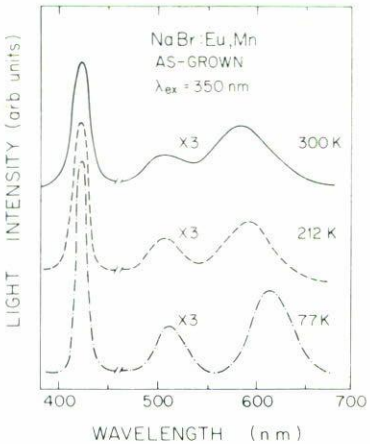

FIGURE 16. Emission spectrum of as-grown NaBr single crystals doubly doped with europium and manganese ions as a fucntion of sample temperature (After Muñoz *et al.* 1987).

b) The system NaBr:Eu:Mn

Very similar results to those described above were found by Rubio, Muñoz and García [51] in sodium bromide crystals codoped with europium and manganese ions.

The optical-absorption spectrum of a doubly doped crystal containing 8 ppm of Eu^{2+} and 130 ppm of Mn^{2+} consisted of two broad bands whose centers of gravity peaked at $\sim$ 40000 and $\sim$ 28900 cm^{-1}. When the crystals were excited with light lying in either of the two broad absorption bands, the fluorescence spectra portrayed in Figs. 16 and 17 for "as-grown" and quenched samples were obtained.

The room-temperature emission spectrum of the as-grown crytals consisted of three bands peaking at 428, 510, and 590 nm. Both the 510 and 590 nm emission peaks shift to lower energies (longer wavelengths) as the temperature is lowered, whereas the 428 nm emission peak does not appreciably shift. Both the peak energy and shift with temperature of the 510 and 590 nm bands are consistent with Mn^{2+} emission characteristics.

When the as-grown crystals were heated for 1 h at 800 K and then quenched to room temperature, the recorded emission spectrum was found to be different. In particular, the emission band peaking at 510 nm disappeared after the thermal treatment. Moreover, the intensity of the orange band increased at the expense of the europium emission band peaking at 428 nm, and its wavelength postion shifted from 590 to 585 nm. The evolution of the intensities of the emission bands peaking at 428, 510, and $\sim$ 590 nm as a function of the annealing temperature to which the as-grown crystal was subjected is portrayed in Figs. 18(a) and 18(b). In order to obtain these data the crystal was heated for 30 min at the temperatures given in the figure and then quenched to room temperature to record the emission spectrum.

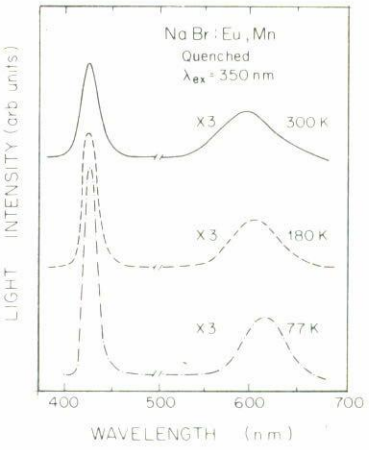

FIGURE 17. Emission spectrum for quenched NaBr single crystals doubly doped with europium and manganese ions as a function of sample temperature (After Muñoz *et al.* 1987).

In order to get additional information on the processes taking place during the annealing treatments, EPR measurements were also performed in parallel with the optical ones. Previous to any heat treatment, the spectrum of the as-grown crystal mainly consisted of an isotropic broad line (Fig. 19). A weak Eu^{2+} spectrum due to those europium ions occupying C_{2v} symmetry sites in the lattice of NaBr [51] [*i.e.*, associated with sodium cation vacancies along ⟨110⟩ directions forming impurity $(I - V)$ dipolar complexes] was also detected. The broad line had a Lorentzian shape with a full width at half maximum of 300 ± 30 G and a g factor close to 2. This broad line is quite similar to that frequently observed in manganese-doped NaCl and it has been commonly interpreted on the basis of a precipitated state of manganese in the crystalline matrix [52,53].

When the as-grown crystal was heated, the intensities of the Eu^{2+} EPR spectrum, as well as of the broad manganese line changed as illustrated in Figs. 18(a) and 18(b). At this point, it should be pointed out that the broad line did not disappear even after heating the crystal at 800 K for several hours. This result may give an indication that the solubility limit of Mn^{2+} in the lattice of NaBr is below 130 ppm at 800 K.

We show the 77 K excitation spectra corresponding to the 428, 510-, and 590 nm bands observed in the emission spectrum of the as-grown crystals in Fig. 20. In Fig. 21 the excitation spectra for the emission bands peaking at 428 and 585 nm observed in the quenched samples are displayed. In both cases, the intense excitation bands are due to Eu^{2+} transitions. In the excitation spectra of the orange emission, several attempts were made to revolve the Mn^{2+} absorption bands in the overlap region of the Eu^{2+} emission. However, all of them were unsuccessful in view of the presence of the xenon lines of the excitation lamp in this spectral region.

Lifetime measurements were also performed on the emission transitions observed in the as-grown and quenched crystals in the range of tempertures 10–300 K. The re-

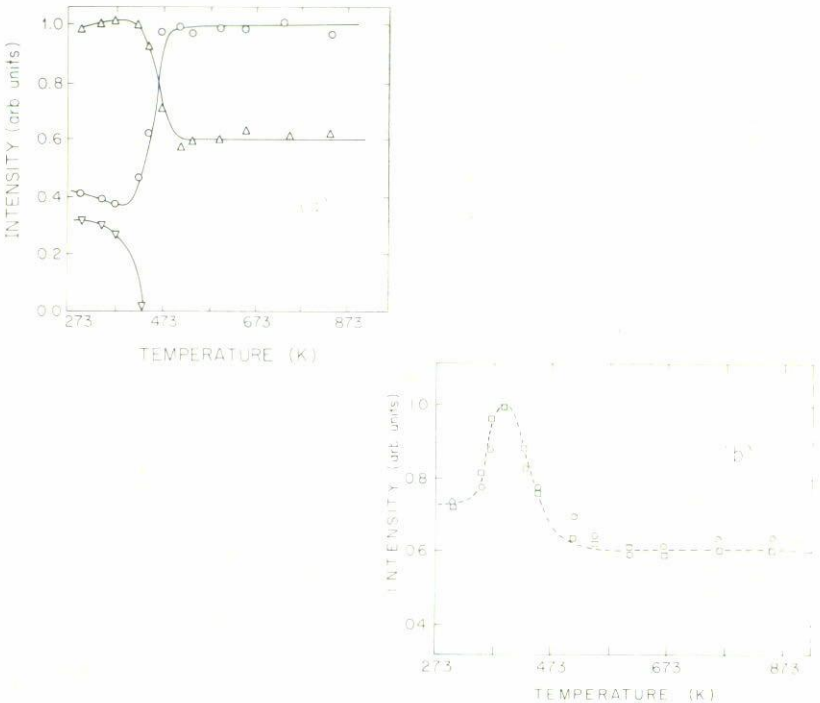

FIGURE 18. (a) Evolution of the intensities of the broad manganese EPR line (Δ), the 510 nm emission band (∇), and of the orange manganese emission band peaking at 590 nm (0) as a function of the temperature to which the as-grown crystal of *NaBr* was subjected. (b) Evolution of the intensities of the Eu^{2+} EPR spectrum (DA) and of the emission band peaking at 428 nm (0) (After Muñoz *et al.* 1987).

sults obtained are given in Figs. 22(a) and 22(b) for as-grown and quenched samples, respectively. In this temperature range, the manganese relaxation signal obtained in the quenched crytals appeared as a pure exponential decay with a time constant which corresponds to the lifetime of the $^4T_{1g}(G)$ excited level of Mn^{2+} . The decay scheme of the Eu^{2+} fluroescence consisted of a unique decay constant the value of which is 1.05 ± 0.04 μs at room temperature and it was practically independent of temperature in the range 10–300 K as can be appreciated from the results portrayed in Fig. 22. The Eu^{2+} fluorescence in a sample having no manganese present also exhibited a pure exponential decay in the range of temperatures 10–300 K with a time constant which was determined to be equal, within experimental error, to that measured for the Eu^{2+} emission in the doubly doped crystal. These data are also included in Fig. 22 for the sake of comparison.

The decay scheme of the Eu emission in the as-grown crystals was found to be nearly identical to that found in the quenched samples. However, the Mn^{2+} emission at 590 nm appeared as a non-exponential decay with the first e^{-1} time equal to

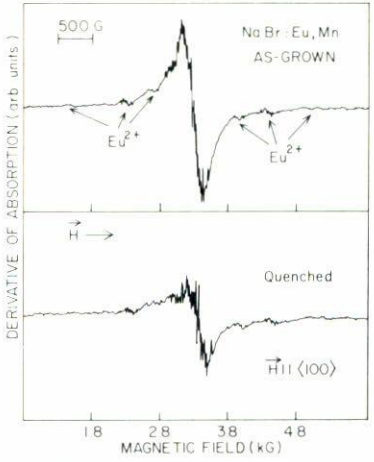

FIGURE 19. Room temperature EPR spectrum observed for as-grown and quenched samples of NaBr (After Muñoz *et al.* 1987).

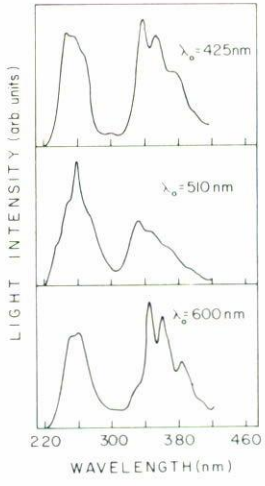

FIGURE 20. Liquid nitrogen excitation spectra corresponding to the emission bands peaking at 428, 510 and 590 nm in as-grown crystals of NaBr (After Muñoz *et al.* 1987).

$\sim$ 4 ms at room temperature. This value increased as the sample temperature was lowered from 300 to 10 K. The luminescence of the emission band peaking at 510 nm also appeared as a non-exponential decay with the first e^{-1} time equal to $\sim$ 0.2 ms; this value being slightly temperature dependent.

The presence of the Eu^{2+} absorption bands in the excitation spectrum of the orange manganese emission in as-grown and quenched crystals indicate that energy transfer from europium to manganese ions occurs in both cases. The intensity of

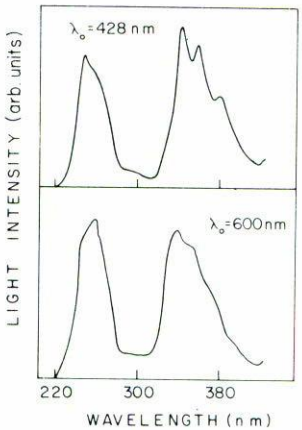

FIGURE 21. 77 K excitation spectra of the 428 and 585 nm emission bands observed in quenched crystals of NaBr (After Muñoz *et al.* 1987).

the Mn^{2+} emission observed in the quenched samples is much greater than can be explained by energy transfer between statistically distributed impurity ions. In fact, for the low Eu^{2+} concentration in the employed samples, the interaction distance between the sensitizer europium ions and the activator manganese ions is so large for statistically distributed impurities, that energy transfer would have to be extremely efficient over this range since the experimentally determined rise time of the manganese luminescence is quite short (< 50 ns). If a preferential pairing of the Eu and Mn ions in the NaBr lattice occurred, then considerable sensitization would result even at low concentrations of both types of ions. This pairing may be expected in the sodium bromide lattice. In fact, if these two ions couple through a Br ion along a ⟨100⟩ direction, then they must fit quite well into a space of 5.96 Å.

For an interaction distance between europium and manganese ions of 5.96 Åin the NaBr lattice, energy transfer may proceed at a rapid rate which quenches the sensitizer luminescence completely. This conclusion is supported by the lifetime data portrayed in Fig. 22 which show that the Eu^{2+} lifetimes of NaBr:Eu:Mn and NaBr:Eu are the same within experimental error.

From the optical and lifetime data mentioned above for the copper-quenched crystals the ratio for the number of europium ions which are paired with the manganese ions (N_{sp}) and the total concentration of europium ($N_{st} = N_{si} + N_{sp}$) in the crystal was obtained in the same manner as above for the NaCl:Eu:Mn system the result being $N_{sp}/N_{st} = 0.27$. This result is in very good agreement with the ionic radius criterion proposed by Rubio and coworkers to predict pairing between two doubly valent impurity ions in an alkali halide host between which energy transfer is desired.

On the other hand, pulse excitation of the low-energy Eu^{2+} absorption band resulted in a Mn^{2+} luminescence with a rise time shorter than 50 ns. Substituting

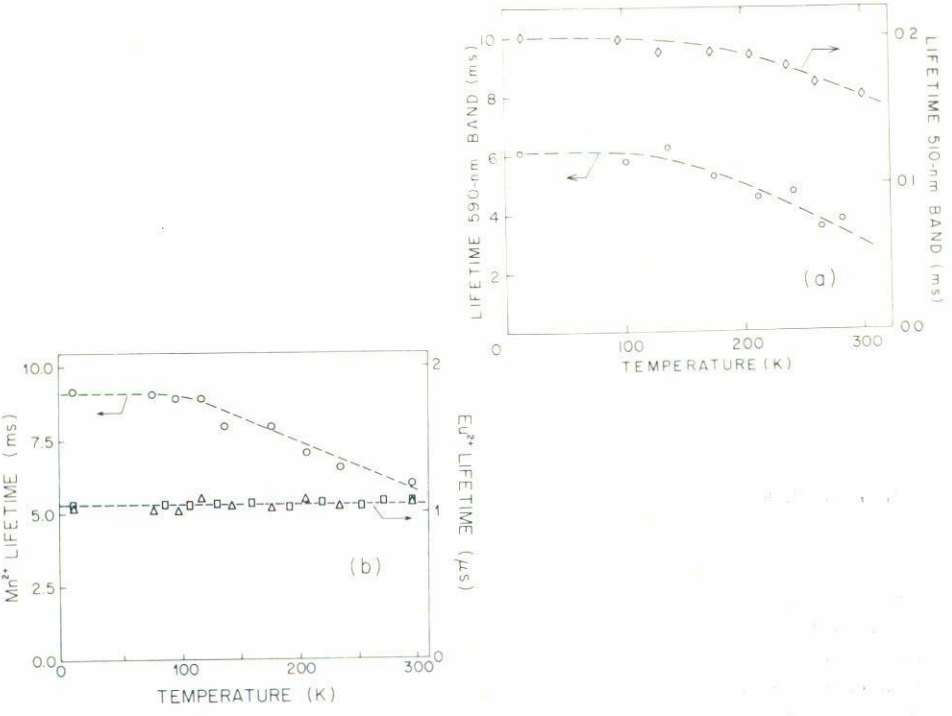

FIGURE 22. (a) Lifetime data for the 510 and 590 nm emission bands as a function of sample temperature in as-grown samples of NaBr. (b)Lifetimes of the 428 (Δ) and 585 nm (0) emission bands as a function of sample temperature in quenched samples of NaBr. Lifetime data for the Eu-emision (DA) in NaBr:Eu are also included for the sake of comparison (After Muñoz *et al.* 1985).

the experimentally determined values for t_{max}, and β_a in Eq. (15), it is obtained that $W_{DA} \gg 3 \times 10^9$ s^{-1}

The possible mechanism for the $Eu^{2+} \rightarrow Mn^{2+}$ energy transfer in NaBr was also analyzed by Rubio *et al.* [50] and Muñoz [54] using Dexter's theory of energy transfer and the dimer configurations given in Fig. 15. The obtained values for W_{DA}(DD) and W_{DA}(DQ) are given in Table III along with those obtained for the NaCl:Eu:Mn system. The closer agreement between the calculated values for W_{DA} and that estimated experimentally from the measure of the rise time of the Mn^{2+} emission after pulse excitation of Eu^{2+}, is achieved when the ⟨100⟩ dimer configuration (D_1) is performed for the calculations. Moreover, it appears that Eu→Mn energy transfer via a superexchange interaction mechanism has a higher probability than Eu→Mn energy transfer via a multipolar interaction mechanism.

c) The systems NaI:Eu:Mn *and* KCl:Eu:Mn

Very recently, Camarillo and Rubio [55] and Rubio and coworkers [56] analyzed the energy transfer taking place from Eu^{2+} to Mn^{2+} ions in NaI and KCl crystals in order to obtain additional evidence which may give support for the ionic radius criterion to predict impurity pairing in the alkali halide lattices.

Since the obtained results by Camarillo and Rubio in the system NaI:Eu:Mn are very similar to those described above for NaCl and NaBr, they will not be presented here for the sake of brevity. The reader interested in those results should referred to the literature. It is important to point out, however, that the energy transfer from Eu^{2+} to Mn^{2+} ions found in the acetone quenched crystals of NaI also occurred between the europium and manganese close pairs which were preferentially formed in the lattice; the value for N_{sp}/N_{st} being ~ 0.10 in agreement with the expectation of the ionic radius criterion.

On the other hand, fluorescence intensity and lifetime measurements of the Eu^{2+} and Mn^{2+} emissions carried out in single crystals of KCl codoped with europium and manganese ions indicated that sensitized luminescence with the europium ions as sensitizers and the manganese ions as activators occurred between Eu^{2+}-Mn^{2+} pairs; the number of these pairs being, however, quite smaller than those formed in the sodium halide lattices.

The absorption of Eu^{2+} ions in a doubly doped crystal of KCl is illustrated in Fig. 23 for as-grow and quenched samples. When the cyrstals are illuminated with light having the appropriate wavelengths for absorption in the ultraviolet bands shown in Fig. 23, luminescence is observed. This spectrum is shown in Fig. 24 for an "as grown" crystal as a function of sample temperature. It should be noted that the 590 nm emission peak energy shifts to lower energy as the temperature is lowered, whereas the 419 nm emission peak energy does not appreciably shift. The shift with temperature of the red emission is consistent with Mn^{2+}-emission characteristics. On the other hand; the 419 nm emission is due to the $4f^6 5d(t_{2g}) \rightarrow 4f^7(^8S)$ transition of the europium ions.

Thermal quenching of the "as-grown" crystals produced a significant increase in the signal intensity of the blue emission and a drastic reduction of the red one. The obtained fluorescence spectrum of a freshly quenched crystal is portrayed in Fig. 25. The inset in this figure shows the excitation spectrum for the emission at 590 nm. The intense excitation bands are those due to Eu^{2+} transitions.

Lifetime measurements in the range of temperatures (77–300 K) were also carried out on the blue and red emission transitions observed in the spectrum of the quenched crystals. In this temperature range, the manganese relaxation signal appeared as a pure exponential decay with a time constant which corresponds to the lifetime of the $^4T_{1g}(G)$ excited level of Mn^{2+}. On the other hand, the decay time increased continuously from 28 ms at room temperature to 51 ms at liquid nitrogen temperature. The decay scheme of the Eu^{2+}-fluorescence consisted of a unique decay constant the value of which was found to be 1.2μs at room temperature and it was practically independent of sample temperature. The Eu^{2+}-fluorescence in a sample having no manganese present also exhibited a pure exponential decay in the range

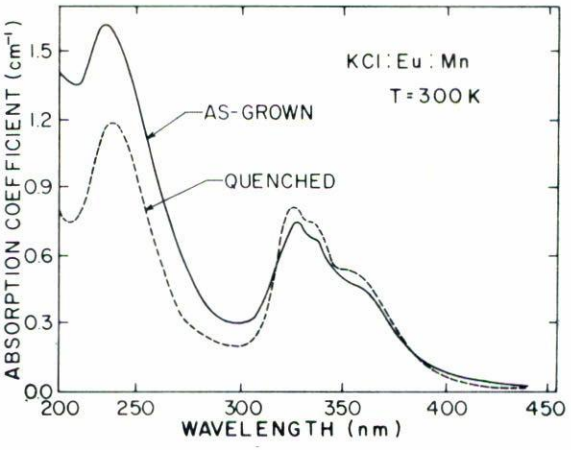

FIGURE 23. Absorption spectra at 300 K for a KCl:Eu:Mn crystal containing 10 ppm Eu^{2+} and 120 ppm Mn^{2+} in as-grown and quenched samples (After Rubio *et al.* 1988).

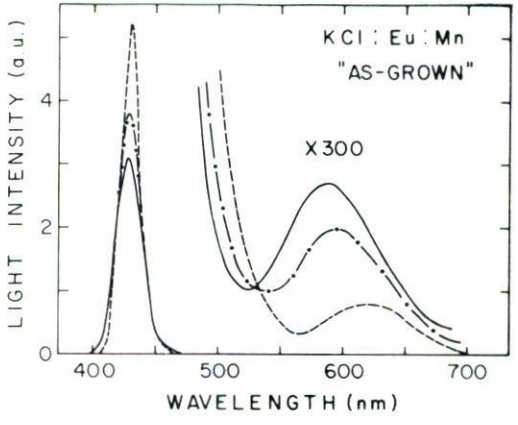

FIGURE 24. Emission spectra for the same as-grown crystal used for the data in **Fig. 23 as a** function of sample temperature (After Rubio *et al.* 1988).

of temperatures (77–300 K) with a time constant which was determined to be equal, within experimental error, to that measured for the Eu^{2+} emission in the quenched doubly doped crytals.

When the quenched crystals were stored at room temperature, the intensity of the red emission increased at the expense of that of europium. In order to get additional information of the processes taking place during the annealing treatment at this particular temperature, EPR measurements were carried out in parallel with

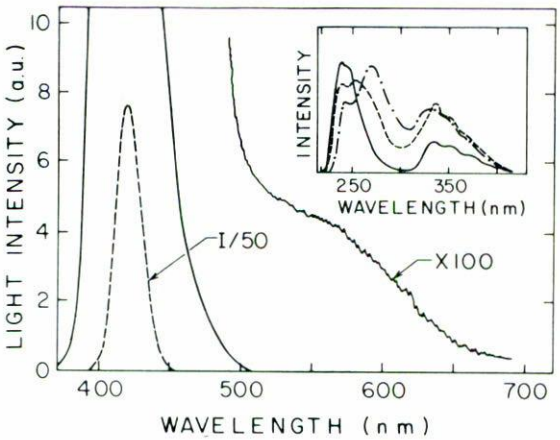

FIGURE 25. Room temperature emission spectrum of an acetone quenched sample of KCl when the excitation is performed at 330 nm. The inset displays the excitation spectra for the red emission band observed in quenched (—) and annealed samples at 300 (- - -) and 473 K (- · -) for 20 days (After Rubio *et al.* 1989).

the optical ones. The observed EPR spectrum of a quenched sample was the superposition of three different spectra. One of them was due to Eu^{2+} ions associated with a nearest neighbor cation vacancy forming $(I-V)$ dipolar complexes, while the other two were due to Mn^{2+} ions associated with nearest and next nearest cation vacancies (spectra III_1 and III_2, respectively in Watkin's notation [57]). The intensities of all these spectra decreased as a function of the annealing time at room temperature; the decrease in the EPR signal intensity due to Eu^{2+}-dipolar complexes being closely correlated with the decrease in the intensity of the Eu-emission peaking at 419 nm as can be appreciated from the results given in Fig. 26. In parallel with the reduction in the concentration of the Eu^{2+} and Mn^{2+}-cation vacancy dipoles, the intensity of the emission band peaking at 590 nm increased. Also, a broad band was found to grow in the central part ($g \sim 2$) of the EPR spectrum, suggesting that manganese aggregation (precipitation) was taking place. Similar results were found when the crystals were annealed at 473 K. In this case, however, the increase in the intensity of the manganese emission and the decrease in the Eu^{2+} and Mn^{2+}-dipolar concentration occurred in shorter times. The excitation spectra of the red emission band observed in the crystals which were annealed at either 300 or 473 K are also portrayed in Fig. 25 for the sake of comparison.

The presence of the Eu^{2+}-absorption bands in the excitation spectrum of the organge manganese emission in "as-grown" and quenched crystals of KCl indicates that energy transfer from europium to manganese ions occurs in both cases. This process is expected to occur in KCl since the Eu^{2+} emission overlaps considerably the Mn^{2+} absorption in this crystal as an be seen from the spectra portrayed in

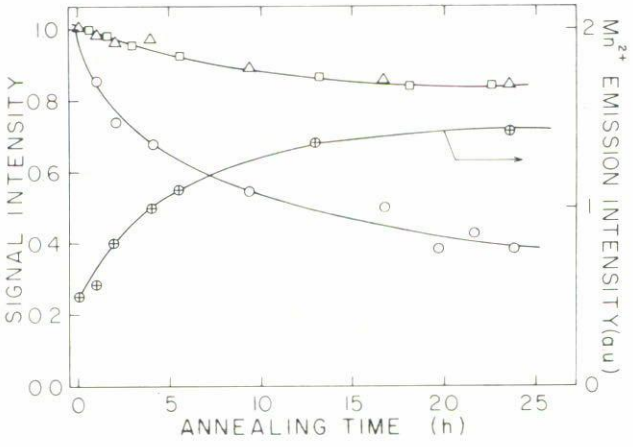

FIGURE 26. Impurity-vacancy dipole decays in quenched KCl:Eu:Mn as a function of the annealing time at 300 K. The symbol Δ illustrate the decay of the Eu emission, the symbol DA the decay of the EPR Eu-signal intensity. The symbol 0 depicts the decay of nearest neighbor Mn^{2+}-cation vacancy dipoles as measured by EPR while the symbol $\oplus$ illustrates the growth of the red emission band (After Rubio *et al.* 1988).

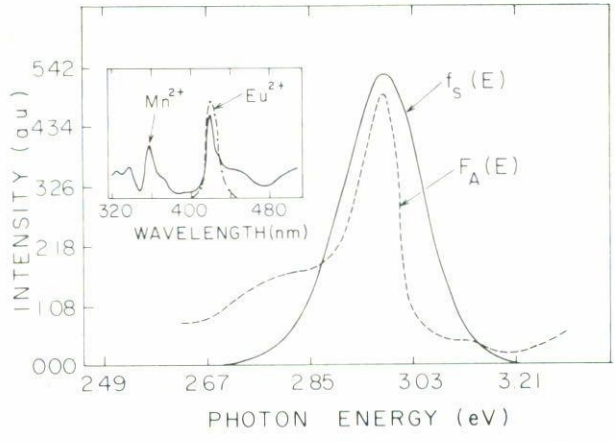

FIGURE 27. Normalized line-shape functions for the Eu-emission $[f_s(E)]$ and Mn-absorption $[F_A(E)]$. The inset shows the overlap region of the Eu-emission and the Mn^{2+} absorption in KCl. The latter was taken from Mehra and Venkateswarlu (Ref. [58]).

Fig. 27. The Mn^{2+}-absorption spectrum portrayed in this Fig. was taken from the work of Mehra and Venkateswarlu.

For the low concentration of Eu^{2+} and Mn^{2+} ions in the samples, the interaction distance between sensitizers and activators calculated from a truly random

distribution of the impurities is quite large to expect that energy transfer should not occur in the freshly quenched crystals. Moreover, the energy transfer would have to be extremely efficient over the large interaction distance since the rise time of the Mn^{2+} luminescence after pulse excitation of Eu^{2+} was found to be shorter than 30 ns. If a preferential pairing of the sensitizer and activator occurred in the lattice of potassium chloride, then considerable sensitizaiton would result even at low concentration of both types of ions.

From the experimentally determined data described above, the value for N_{sp}/N_{st} was found to be ~ 0.002, indicating therefore, that only 0.2% of the europium ions were paired with the manganese ions in the quenched crystals of KCl. This finding is in contrast with those reported for the sodium halide lattices in which a larger fraction of the europium ions were found to be paired with the manganese ions even after an efficient quench in acetone. It is, however, in agreement with the expectation of the ionic radius criterion. In fact since the ionic radii of Eu^{2+} and Mn^{2+} are smaller than that of K^+ , it is expected that the Eu-Mn pairs do not fit well in the alloted space in the lattice of KCl (6.28Å), and therefore the strain induced by the presence of the donor and acceptor alone may not be significantly reduced by the formation of these pairs.

The analysis [54] of the possible mechanisms for energy transfer from europium to manganese ions in the lattice of KCl indicated that the energy transfer via a superexchange interaction mechanism has a higher probability than energy transfer via a multipolar interaction mechanism. Moreover, it was also found that the D_1 dimer configuration portrayed in Fig. 15 is the most appropriate one in order to occur the energy transfer between these two impurities. Table III gives values for the rate of energy transfer using different types of interaction mechanisms and dimer complexes.

d) The system NaCl:Sn:Mn

In order to obtain additional information which may give support to the ionic radius criterion to predict pairing between doubly valent impurity ions in an alkali halide host, Muñoz and Rubio [59] performed, very recently, a detailed study of Sn^{2+}-sensitized Mn^{2+} fluorescence in monocrystalline NaCl. Tin was selected to perform this investigation since the optical absorption and emission spectra of this ion in NaCl has been previously characterized [60] as a function of concentration as well as of several thermal treatments given to the crystals. Moreover, its ionic radius (0.93 Å) was quite appropriate to make a useful comparison with the data obtained in NaCl doubly doped with either europium and manganese or lead and manganese ions.

The room temperature absorption spectrum of a quenched sample of NaCl containing 28 ppm of Sn ion is portrayed in Fig. 28. It consists of three structured bands labeled *A*, *B* and *C* in increasing order of energy. These bands are due to electronic transitions [61,62] of the Sn^{2+} ions associated with the change in configuration $s^2 \rightarrow sp$; the *A* band has been attributed to the spin-orbit allowed transition $|^1A_{1g}\rangle \rightarrow v|^1T_{1u} + \mu|^3T_{1u}\rangle$ where μ and v are the mixing coefficients for the $|^3T_{1u}\rangle$

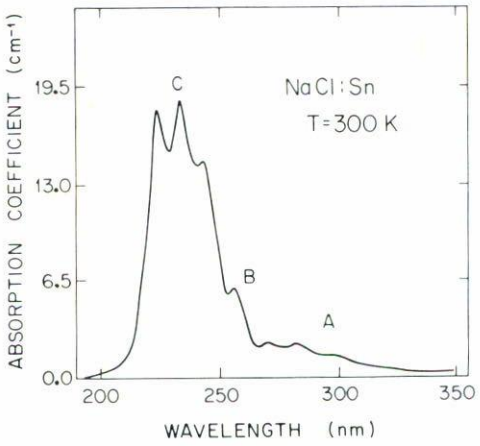

FIGURE 28. 300 K absorption spectrum for a freshly quenched crystal of NaCl containing 28 ppm of Sn^{2+} ions (After Muñoz and Rubio 1988).

and $|^1T_{1u}\rangle$ states; the B band to the forbidden transitions $|^1A_{1g}\rangle \rightarrow |^3T_{2u}\rangle$ and $|^1A_{1g}\rangle \rightarrow |^3E1u\rangle$ and the C band to the transition $|^1A_{1g}\rangle - \mu|^1T_{1u}\rangle + v|^3T_{1u}\rangle$.

Luminescence was observed when the crystals were illuminated with light lying within either of the A, B or C bands. Fig. 29(a) shows, as an example, the obtained emission spectrum when the excitation was performed at 266 nm and for two selected sample temperatures. A similar spectrum was found when the excitation was performed with light lying in the wavelength range 230–320 nm. The room temperature emission spectrum consists of a broad band peaking at 440 nm. When the sample temperature was lowered to 77 K, the width of the 440 nm band decreased considerably and another band peaking at 530 nm became apparent in the emission spectrum. This latter band was hardly detectable in the slightly tin-doped crystals (< 15 ppm) after a quenching treatment. The intensity ratio between the 530- and 440 nm bands was found to increase with tin concentration, as well as with the room-temperature storage of the freshly quenched crystals. For a tin concentration of $\sim$ 150 ppm, the intensities of both bands were found to be comparable in the emission spectrum of the quenched crystals; all these results being in good agreement with previous data. [60]

Although several models have been proposed to explain the origin of these two tin emission bands, the situation is far for being clear. While Zazubovich [63,66] and co-workers attributed these bands to the coexistence of different types of isolated Sn cation vacancy centers (*i.e.*, the 440 nm band was ascribed to tin ions associated with a next nearest-neighbor cation vacancy and the 530 nm band with the tin ions associated with a nearest-neighbor cation vacancy), Fukuda [67,69] proposed that these two emissions are due to transitions from the two kinds of minima (A_T and A_X) on the adiabatic potential-energy surface (APES) of the $^3T_{1u}$ relaxed excited state of the isolated tin ions which are forming the Sn^{2+} cation vacancy dipoles. The

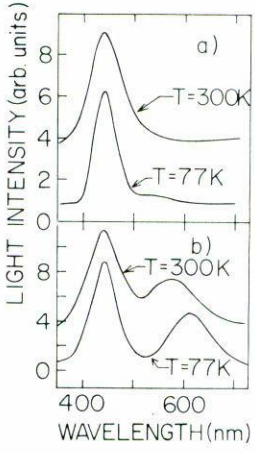

FIGURE 29. (a) Emission spectra for Sn^{2+} in NaCl at two selected sample temperatures. (b) Emission spectra for a tin and manganese doubly doped quenched crystal of NaCl when the excitation is performed at 266 nm (After Muñoz and Rubio (1988).

coexistence of these two minima was attributed [67] to the quadratic Jahn-Teller effect and/or anharmonicity or to spin-orbit mixing between the excited states $^3T_{1u}$ and $^1T_{1u}$. On the other hand, Marculescu *et al.* [60] proposed that the origin of these two bands could be alternatively explained considering that the A_T (440 nm) emission is produced by deexcitation of a tin center in the $^3T_{1u}$ state while the A_X (530 nm) emission is produced by deexcitation of a different tin center which reached the excited state $^1T_{1u}$ through a resonant energy-transfer process from a tin center in the excited state $^3T_{1u}$. Moreover, since the intensity of the 530 nm band is enhanced with the increase in tin concentration, as well as with the room-temperature storage of the samples, it is suggested that this emission is related in some way to tin aggregated complexes which are formed as a result of the aging at 300 K or because the tin concentration in the crystal is above the solubility limit.

In view of this situation and because the presence of a significant concentration of tin aggregates in the samples analyzed might complicate the interpretation of the results obtained, all the data reported below were taken on slightly tin-doped crystals for which the emission peaking at 530 nm was hardly detectable even under very high-resolution conditions of the employed experimental setup.

On the other hand, the absorption spectrum of a tin (4 ppm) and manganese (30 ppm) doubly doped quenched crystal of NaCl was found to be nearly identical to that portrayed in Fig. 28 for the tin-doped NaCl. Light absorption in either of the A, B, or C bands produced an emission which is shown in Fig. 29(b) for two selected sample temperatures. At both temperatures the emission spectrum consisted of only two broad bands situated in the blue and red regions of the electromagnetic spectrum. The blue emission had the same characteristics (peak position and width)

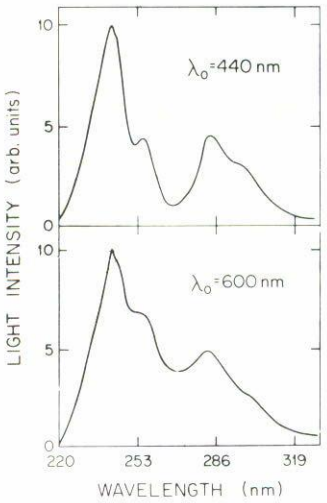

FIGURE 30. 77 K excitation spectra for the emission bands peaking at 440 and 600 nm (After Muñoz and Rubio 1988).

of the tin-emission band peaking at 440 nm in NaCl:Sn and therefore, was related with the deexcitation of the tin ions in the doubly doped quenched crystals. On the other hand, the red emission was observed only after the NaCl:Sn crystal was contaminated with manganese ions. The peak position of this emission was found to shift to the red region of the electromagnetic spectrum when the sample temperature was lowered. Both the peak energy and shift with temperature of this emission are consistent with the Mn^{2+} emission characteristics. Moreover, the introduction of manganese ions into the tin-doped NaCl crystals produced a reduction in the integrated intensity of the tin emission.

The liquid-nitrogen excitation spectra for the emission bands peaking at 440 and 600 nm are portrayed in Fig. 30. In all cases, the intense excitation bands are due to Sn transitions.

Lifetime measurements were carried out in the range of temperatures 11–300 K on the tin and manganese emission transitions peaking at 440 and 580–620 nm, respectively. The very small intensity of the tin emission peaking at 530 nm in all the samples analyzed did not allowed to obtained accurate lifetime data for this emission. In the temperature range investigated the manganese fluorescence decay exhibited a purely exponential time dependence with a no observable rise time. The time constant of the decay which corresponds to the lifetime of the $^4T_{1g}(G)$ excitation level of Mn^{2+} increased from 18.5 ms at room temperature to 37 ms at 11 K. The tin fluorescence peaking at 440 nm also consisted of a unique decay constant which increased from 2.3μs at room temperature to 29μs at 11 K unlike the non-exponential decays usually observed for ion-ion energy transfer in solids. On the other hand, the Sn^{2+} fluorescence peaking at 440 nm in a sample having no manganese present also exhibited a pure exponential decay with a lifetime which

was determined to be equal, within experimental error (±5%), to that measured for the Sn^{2+} emission in the doubly doped crystals.

It was also ascertained that the aging at room temperature for several months did not produce a significant change in either the intensity of the tin emision or of the manganese one. This result might be expected considering that for the low concentrations of donor and acceptor ions in the samples employed it is quite certain that the room temperature solubility limit of these two impurities has not been exceeded. Therefore, impurity aggregates and/or precipitates are not expected to be formed during the room-temperature annealing.

The more significant experimental data described above can be summarized as follows:

(1) Room-temperature excitation of the Sn^{2+} ions in the slightly doped NaCl:Sn (4 ppm), Mn^{2+} (30 ppm) samples produced two emission bands peaking at 440 and 580 nm. The former band is due to the deexcitation of the tin ions, while the latter is due to the transition $^4T_1(G) \rightarrow {}^6A_1$ of the Mn^{2+} ions. The peak position of this band moves to the red when the sample temperature decreases because of an increase in the magnitude of the crystal field acting at the site occupied by the manganese ions. The decrease in the lifetime of this emission when the sample temperature is increased may be explained considering that the probabilities for the phonon-assisted and nonradiative processes are enhanced with the increase in temperature.

(2) The excitation spectrum of the Mn^{2+} luminescence reveals the presence of the Sn^{2+} absorption bands. This result clearly indicates that $Sn^{2+} \rightarrow Mn^{2+}$ energy transfer takes place in the doubly doped quenched samples of NaCl. This process occurs even for the very low concentrations of the donor and activator ions in our crystals.

(3) Pulse excitation of Sn^{2+} resulted in a Mn^{2+} luminescence with no observable rise time. Taking into account the sensitivity and the overall time response of the employed experimental setup, this result indicated that the rise time of the manganese fluorescence was shorter than 25 ns.

(4) The decay pattern of the Sn^{2+} luminescence in NaCl:$Sn^{2+}$is not affected by the presence of manganese ions in the doubly doped crystals.

(5) The total integrated emission of the Sn^{2+} ions is reduced by the presence of the manganese ions.

The Sn^{2+} emission overlaps considerably the Mn^{2+} absorption as can be appreciated from the spectra portrayed in Fig. 31. This spectral overlap is a necessary condition for the occurrence of $Sn^{2+} \rightarrow Mn^{2+}$ energy transfer. However, for the low concentrations of the impurities in the samples, the interaction distance between donors and acceptors calculated from a truly random distribution of the impurities is found to be > 100 Å. At this large interaction distance energy transfer between the impurities should not occurred in the doubly doped quenched crystals. In fact, the rate of Sn→Mn energy transfer calculated from Dexter's theory of energy transfer, at a distance of ~ 100 Å, is found to be quite small compared with the experimentally determined intrinsic decay rate of the Sn^{2+} ions. Therefore, the observation of tin-sensitized manganese fluorescence in the samples employed suggests that the

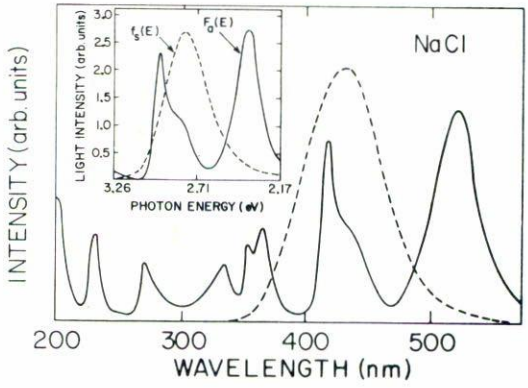

FIGURE 31. Room temperature overlap region of the tin emission (dashed line) and manganese absorption (solid line). The latter spectrum was taken from the work of Rodríguez *et al.* (Ref. 29) The inset shows the normalized line-shape functions in the overlap region.

impurities are not randomly distributed in the lattice but rather occur as coupled pairs of Sn^{2+}-Mn^{2+}. A nearest-neighbor cation separation distance (~ 5.6 Å) in the NaCl lattice along the [100] direction predicts a very efficient energy transfer, as it will be shown below.

The essential features of the kinetics of Sn→Mn energy transfer in NaCl can be described by the model depicted in Fig. 13. Considering that the radiative decay rates are equal to the inverse of the low temperature (11 K) lifetime values ($\beta^r_{si} = 3.4 \times 10^4 s^{-1}$, $\beta^r_a = 27 s^{-1}$) it is found from Eq. (13) that $N_{sp}/N_{st} \sim 0.05$ when the experimentally determined room temperature data *i.e.*, $\beta_{si} = 4.3 \times 10^5 s^{-1}$, $\beta_a = 54 s^{-1}$ and $\frac{I_a}{I_{si}} \cong 0.3$ are employed in Eq. (13). Thus, about 5% of the total concentration of the Sn^{2+} ions in the doubly doped quenched crystals are paired with the manganese ions.

However, taking into account that pulse excitation of Sn^{2+} resulted in manganese fluorescence with a rise time shorter than 25 ns, it is found from Eq. (15) that the rate of $Sn^{2+} \rightarrow Mn^{2+}$ energy transfer is $> 3 \times 10^8 s^{-1}$ at 300 K.

Considering the forbidden nature of the $3d \rightarrow 3d$ Mn^{2+} absorption, it is expected that the Sn→Mn energy transfer mechanism which takes place between these two impurity ions in NaCl is either of the electric dipole-quadrupole type or exchange in nature. Since the exact nature of the Sn-Mn pair cannot be inferred from the experimentally determined optical data described above, the rate of energy transfer via a dipole-quadrupole interaction mechanism was calculated using different configurations for the Sn-Mn dimer complex such as those given in Fig. 15. The obtained values for $W_{DA}(DQ)$ for each of the considered dimer complexes are given in Table III. In the same table the rate of energy transfer calculated from the

use of an electric dipole-dipole interaction mechanism is also included for the sake of comparison. As expected, more reasonable values are obtained when a dipole-quadrupole interaction mechanism is employed rather than an electric dipole-dipole one. Moreover, the closer agreement between the calculated values of $W_{DA}(DQ)$ and that estimated experimentally is achieved when the [100] dimer configuration is employed to perform the calculations. The calculated value, however, is still smaller than that estimated from the experimental data. This fact suggests that an exchange (superexchange) interaction mechanism is probably the responsible for the energy transfer from the tin to the manganese ions forming the impurity pair. Using the D_1 dimer configuration, a value for R_c ($\sim$ 10 Å) similar to that found for the dipole-quadrupole interaction mechanism and a typical value for the "effective Bohr radius" of 1.3 Å, which is about half the manganese chlorine separation distance in this dimer configuration, a rate of 0.3×10^9 s^{-1} is obtained. If one juxtaposes this result to the $W_{DA}(DQ)$ calculated above, it may be concluded that Sn→Mn energy transfer via a superexchange interaction mechanism appears to have a higher probability than Sn→Mn energy transfer via a multipolar interaction mechanism. An estimation of the rate of energy transfer via an exchange mechanism is not simple for the case in which the impurities are forming the other dimer configurations as those shown in Fig. 15. However, the large distances between donor and acceptor ions, as well as their locations in these complexes appear to be unappropriated for the occurrence of this type of interaction.

Finally, in order to obtain more information which may give additional support to the validity of the ionic radius criterion to predict impurity pairing in an ionic solid, experiments are now in progress in our laboratory using the systems NaCl:Cu^+:Mn^{2+}, CaF_2:Ce^{3+}:Mn^{2+}, CaF_2:Eu^{2+}:Mn^{2+} and $CaCl_2$:Eu^{2+}:Mn^{2+}, for which a preferential impurity pairing is expected to occur. The preliminary experimentally determined data have shown that, in all cases, an efficient energy transfer from the donor (Ce^{3+}, Cu^+,Eu^{2+}) ions to the acceptor Mn^{2+} ion takes place even at very low concentrations of both impurity ions. These results suggest that the donor → acceptor energy transfer takes place between the impurity pairs which are preferentially formed in the crystalline matrixes in agreement with expectation of the ionic radius criterion.

4. Conclusions

Radiationless Energy Transfer processes from Eu to Mn and from Sn to Mn ions have been analyzed in several alkali halide crystals. The spectroscopic data presented above demonstrate that both Eu→Mn and Sn→Mn energy transfer takes place in the impurity pairs, which are preferentially formed in the alkali halide matrixes even after the crystals employed are efficiently quenched into acetone. This finding, which has been traditionally considered to be unfrequently in most studies dealing with energy transfer between impurities in solids, seems to be a quite relevant one in order to design more efficient phosphor and laser systems.

The number of impurity pairs was found to be strongly dependant on the selected alkali halide host crystal. They are more numerous in the sodium than in the potassium halide crystals. This fact is in agreement with the expectation of the ionic radius criterion proposed by Rubio and coworkers to explain the observed preferential impurity pairing. Experiments are now in progress in other type of crystals codoped with different kinds of impurities in order to get additional evidence which may support the validity of the ionic radius criterion.

Acknowledgements

This work was partially supported by Consejo Nacional de Ciencia y Tecnología (CONACyT) and Dirección General de Investigación Científica y Superación Académica (SEP).

References

1. S. Rothschild, *Physik. Z.*, **35** (1934) 557; **37** (1936) 757.
2. T. Förster, *Ann. Physik* **2** (1948) 55.
3. T. Förster, *Z. Elektrochem* **53** (1949) 93.
4. T. Förster, *Z. Naturforsch* **4a** (1949) 321.
5. D.L. Dexter, *J. Chem. Phys.* **21** (1953) 836.
6. M.D. Galanin, *Zh. ETF* **21** (1951) 126.
7. M.D. Galanin, *Trudy FIAN SSSR* **12** (1960) 3.
8. G.W. Robinson and R.P. Frosch, *J. Chem. Phys.* **37** (1962) 1962.
9. G.W. Robinson and R.P.. Frosch, *J. Chem. Phys.* **38** (1963) 1187.
10. T. Förster, *Mod. Quantum Chem.* **93** (1965) 111.
11. A.I. Burshtein, *Teor i Eksp Khimiya* **1** (1965) 563.
12. V. Ya Gamurar, E. Yu Perlin and B.S. Tsukerblat, *Fiz. Tverd. Tela* **11** (1969) 1193.
13. E.D. Trifonov and V.L. Shekhtman, *Phys. Stat. Solidii* **41** (1970) 655.
14. P.J. Botden, *Philips Res. Rep.* **7** (1952) 197.
15. C.C. Klick and J.H. Schulman in *Solid State Physics* **5** (1955) 97; F. Seitz and D. Turnbull Ed. Academic Press, N.Y.
16. M. Inokuti and H. Hirayama, *J. Chem. Phys.* **43** (1965) 1978.
17. M. Yokota and O. Tanimoto, *J. Phys. Soc. Japan* **22** (1967) 779.
18. L.G. Van Vitert in *Luminescence of Inorganic Solids*, Ed. by P. Goldberg, Academic, New York (1966) 465.
19. M.J. Weber, *Phys. Rev.* **B4** (1971) 2932.
20. M. Trifaj, *Czech. J. Phys.* **5** (1955) 463; **6** (1956) 533; **8** (1958) 510.
21. R.K. Watts in *Optical Properties of Ions in Solids*, Ed. B. DiBartolo, Plenum Press, New York (1975) 307.
22. W.J.C. Grant, *Phys. Rev.* **B4** (1971) 648.
23. J.C. Wright in *Topics of Applied Physics*, Ed. by F.K. Fong, Springer-Verlag, Berlin (1976) 239.
24. R.C. Powell and G. Blasse in *Structure and Bonding* **42** (1980) 43.
25. G. Blasse, *Philips Res. Repts* **21** (1969) 131.
26. M. Yokota and O. Tanimoto, *J. Phys. Soc. Jpn.* **22** (1967) 779.
27. J. Rubio O., H. Murrieta S., R.C. Powell and W.A. Sibley, *Phys. Rev.* **B31** (1985) 59.

28. H. Murrieta S., J. Hernández A., and J. Rubio O., *KINAM* **5** (1983) 75.
29. F. Rodríguez, M. Moreno, F. Jaque and F.J. López, *J. Chem. Phys.* **78** (1983) 73.
30. F.J. López, H. Murrieta S., J. Hernández A., and J. Rubio O., *Phys. Rev.* **B22** (1980) 6428.
31. J. Rubio O., H. Murrieta S., J. Hernández A., and F.J. López, *Phys. rev.* **B24** (1981) 4847.
32. K. Suzuki, *J. Phys. Soc. Jpn.* **16** (1961) 67.
33. J.A. Chapman and E. Lilley, *J. Mater. Sci.* **2** (1967) 567.
34. E. Lilley and J.B. Newkirk, *J. Mater Sci.* **2** (1967) 567.
35. W. Spengler and R. Kaiser, *Phys. Stat. Solidii* **B66** (1974) 107.
36. J.M. Calleja, A. Ruiz, F. Flores, V.R. Velasco and E. Lilley, *J. Phys. Chem. Solis* **41** (1988) 1367.
37. F. Jaque, F.J. López, F. Cussó, f. Mesegner, and F. Agulló-López, *Solid State Comm.* **47** (1983) 103.
38. J. Hernández A., W.K. Cory and J. Rubio O., *J. Chem. Phys.* **72** (1980) 198.
39. D. Curie, C. Barthou and B. Canny, *J. Chem. Phys.* **61** (1974) 3048.
40. S. Koide and M.H.L. Pryce, *Philos. Mag.* **3** (1958) 607.
41. A.K. Mehra, *J. Chem. Phys.* **48** (1968) 4384.
42. G. Muñoz H., and J. Rubio O., *Cryst. Latt. Defects and Amorph. Mats.* (In press).
43. G.C. Taylor, J.E. Strutt and E. Lilley, *Phys. Status Solidii* **(a) 67** (1981) 263.
44. R. Cywinski, R. Fava, M. Manfredi and E. Mugenski, *Phys. Stat. Solidii* **(b) 143** (1987) 433.
45. J. Rubio O., *Phys. Rev.* **B39** (1989) 1962.
46. J. Rubio O., A. Muñoz F., G. Muñoz H. and M.E. López-Morales, *J. Phys. C. (Sol. St. Phys.)* **21** (1988) 2059.
47. N.M. Bannon, J. Corish and P.W.M. Jacobs, *Philos. Pag.* **A6** (1985) 797.
48. P.W. Anderson in *Magnetism* Vol. 1 Eds. G.T. Rado and H. Sush, Academic Press. New York (1963).
49. H. Dornauf and J. Heber, *J. Luminescence* **22** (1980) 1.
50. J. Rubio O., A. Muñoz F., and J. García M., *Phys. Rev.* **B36** (1987) 8115.
51. G. Aguilar S., H. Murrieta S., J. Rubio O., and E. Muñoz P., *J. Chem. Phys.* **62** (1975) 1197.
52. G.D. Watkins, *Phys. Rev.* **113** (1959) 79.
53. J. Rubio O., A. Muñoz F., and Marco Patrón, *Solid State Comm.* **55** (1985) 109.
54. A. Muñoz F., Ph. D. Thesis (unpublished). UAM-Iztapalapa (1988).
55. E. Camarillo and J. Rubio O., *J. Phys. Condensed Matter* **1** (1989) 4873.
56. J. Rubio O., A. Muñoz F., C. Zaldo and H. Murrieta S., *Solid State Comm.* **65** (1988) 251.
57. G.D. Watkins, *Phys. Rev.* **113** (1959) 79.
58. A. Mehra and P. Venkateswarlu, *J. Chem. Phys.* **45** (1966) 3381.
59. A. Muñoz F., and J. Rubio O., *Phys. Rev.* **B38** (1988) 9980.
60. L. Marculescu, G. Ghita and L. Mihut, *Phys. Stat. Solidii* **(a) 61** (1980) 497.
61. A. Ranfagni, D. Mugnai, M. Bacci, g. Viliani and M. Fontana, *Adv. Phys.* **32** (1983) 823, and references cited therein.
62. A. Fukuda, *Sci. Light (Tokio)* **13** (1964) 64.
63. E. Vasilichenko, S.G. Zazubovich and H.E. Luschik, *Opt. Spectrosk* **32** (1972) 749.
64. E. Realo and S.G. Zazubovich, *Phys. Stat. Solidii* **(b) 57** (1973) 69.
65. S.G. Zazubovich, *Opt. Spectrosk*, **37** (1974) 711.
66. V. Hizhnyakov and S.G. Zazubovich, *Phys. Stat. Solidii* **(b) 86** (1978) 733.
67. A. Fukuda, *Phys. Rev.* **B1** (1970) 4161.
68. A. Fukuda, *Phys. Rev. Letts.* **26** (1971) 314; ibid **28** (1972) 1032.
69. A. Fukuda, *Sol. St. Communications* **12** (1973) 1039.

Resumen. El fenómeno de transferencia de energía no radiativa entre impurezas en sólidos constituye actualmente uno de los problemas fundamentales en la física de la materia condensada en vista de su importancia en una gran variedad de aplicaciones tecnológicas. En el presente artículo se presenta una revisión del trabajo más importante que ha llevado a cabo el autor y sus colaboradores en este campo de investigación. Se reporta que ciertas impurezas, dependiendo de la red cristalina, tienden a formar parejas entre las cuales ocurre un eficiente proceso de transferencia de Energía no radiativo. Este apareamiento preferencial que frecuentemente se ha considerado improbable puede ser de utilidad para diseñar dispositivos ópticos de conversión de luz ultravioleta o infrarroja en visible. Para explicar este apareamiento preferencial Rubio *et al.* propusieron un criterio de radio iónico que parece ser extremadamente útil para seleccionar impurezas y redes cristalinas en los cuales se quiera producir procesos de transferencia de energía eficientes.